Stem Cell Reports
Article
ISSCR
OPEN ACCESS

Transplantation of Skin Precursor-Derived Schwann Cells Yields Better Locomotor Outcomes and Reduces Bladder Pathology in Rats with Chronic Spinal Cord Injury

Peggy Assinck,[1,2,12] Joseph S. Sparling,[1,2,6] Shaalee Dworski,[9] Greg J. Duncan,[1,3,13] Di L. Wu,[1] Jie Liu,[1] Brian K. Kwon,[1,5] Jeff Biernaskie,[6,7,8] Freda D. Miller,[9,10,11] and Wolfram Tetzlaff[1,3,4,*]

[1]International Collaboration on Repair Discoveries, University of British Columbia, Vancouver, BC, Canada
[2]Graduate Program in Neuroscience, University of British Columbia, Vancouver, BC, Canada
[3]Department of Zoology, University of British Columbia, Vancouver, BC, Canada
[4]Department of Surgery, University of British Columbia, Vancouver, BC, Canada
[5]Department of Orthopaedics, University of British Columbia, Vancouver, BC, Canada
[6]Hotchkiss Brain Institute, University of Calgary, Calgary, AB, Canada
[7]Alberta Children's Hospital Research Institute, University of Calgary, Calgary, AB, Canada
[8]Faculty of Veterinary Medicine, University of Calgary, Calgary, AB, Canada
[9]Neuroscience and Mental Health Program, Hospital for Sick Children, Toronto, ON, Canada
[10]Department of Molecular Genetics, University of Toronto, Toronto, ON, Canada
[11]Department of Physiology, University of Toronto, Toronto, ON, Canada
[12]Present address: Center for Regenerative Medicine and Institute for Regeneration and Repair, University of Edinburgh, Edinburgh, Scotland, UK
[13]Present address: Jungers Center for Neurosciences Research, Department of Neurology, Oregon Health and Science University, Portland, OR, USA
*Correspondence: tetzlaff@icord.org
https://doi.org/10.1016/j.stemcr.2020.05.017

SUMMARY

Cell transplantation for spinal cord injury (SCI) has largely been studied in sub-acute settings within 1–2 weeks of injury. In contrast, here we transplanted skin-derived precursors differentiated into Schwann cells (SKP-SCs) into the contused rat spinal cord 8 weeks post-injury (wpi). Twenty-one weeks later (29 wpi), SKP-SCs were found to have survived transplantation, integrated with host tissue, and mitigated the formation of a dense glial scar. Furthermore, transplanted SKP-SCs filled much of the lesion sites and greatly enhanced the presence of endogenous SCs, which myelinated thousands of sprouting/spared host axons in and around the injury site. In addition, SKP-SC transplantation improved locomotor outcomes and decreased pathological thickening of bladder wall. To date, functional improvements have very rarely been observed with cell transplantation beyond the sub-acute stage of injury. Hence, these findings indicate that skin-derived SCs are a promising candidate cell type for the treatment of chronic SCI.

INTRODUCTION

At present there are no treatments to improve neurologic function of the injured spinal cord, beyond surgical decompression of the spinal cord and rehabilitation therapy. However, more efficacious treatments are urgently needed to promote long-term repair and recovery after spinal cord injury (SCI) to benefit people living with chronic motor, sensory, or autonomic deficits. Cell transplantation has long been considered a promising potential therapy to fill that niche (Assinck et al., 2017a; Tetzlaff et al., 2011). As a candidate cell for SCI treatment, Schwann cells (SCs) possess many desirable properties that are known to promote regeneration and repair after CNS injury by a variety of possible mechanisms (Assinck et al., 2017a; Boerboom et al., 2017). For example, SCs secrete trophic factors (Hoke et al., 2006) and form cellular conduits, similar to the bands of von Büngner found in a regenerating nerve (Bunge, 1994). These cellular conduits align rostro-caudally and attract and guide the growth of axons into and across the site of SCI (Bastidas et al., 2017; Bunge, 2016). In addition, SCs myelinate regenerating and spared CNS axons, provide neuroprotection (Pearse et al., 2018), and promote axonal growth/plasticity and concomitant functional recovery (Bunge et al., 2017; Wiliams and Bunge, 2012). Finally, because SCs can be harvested from peripheral nerves and expanded *in vitro*, they are well suited for transplantation in the autologous setting.

To generate sufficient cells for autologous clinical application after SCI, peripheral nerve-derived SCs are typically harvested by excising a segment of sural nerve (Anderson et al., 2017). This procedure may result in sensory deficits and carries a risk of painful neuroma formation (Hood et al., 2009). Those deficits/risks could be avoided by using an alternative, more accessible, source of SCs, such as those generated from skin-derived precursors (SKPs). SKPs are resident multipotent stem cells found in the dermis of mammalian skin. Similar to neural crest stem cells, SKPs can be isolated from neonatal/adult rodent and human skin and differentiated *in vitro* to produce SCs, known as SKP-SCs (Toma et al., 2001; for more citations see Supplemental Experimental Procedures). Given that the harvest of skin is less invasive than that of nerve, SKPs may be a better source of SCs for autologous transplantation after SCI.

Previously, we demonstrated in rats that neonatal SKP-SCs generated from rodent skin and transplanted either acutely (immediately) after cervical crush injury or subacutely (1 week) after thoracic contusion into the site of SCI survived and promoted repair and functional recovery (Biernaskie et al., 2007; Sparling et al., 2015). In addition, we found that acute (immediately post-injury) transplantation of SCs isolated from either neonatal rat nerve or skin-derived precursors promote repair and functional recovery after cervical crush injury (Sparling et al., 2015). Here, we took the next logical step and examined their efficacy in the chronic injury setting. This approach is arguably the most clinically relevant and feasible in clinical trials. Chronic transplantation allows for stabilization of neurological function after SCI and any effects are easier to detect. Delaying treatment also gives time for patients to make informed decisions regarding trial participation (Illes et al., 2011) and for the generation of a sufficient number of cells for autologous transplantation. These considerations have been taken into account in the planning of a recent autologous SC trial in the US (Anderson et al., 2017). However, promoting effective CNS repair in the chronic injury setting is challenging, as the few pre-clinical transplantation studies that have been undertaken with different cell types had no or marginal success to establish functional improvements unless the cells were used in combination with other treatments. Here we transplanted neonatal SKP-SCs generated from rat skin directly into the lesion site 8 weeks after thoracic spinal cord contusions in adult rats. To confirm long-term survival and functional outcomes, and exclude adverse effects, we examined locomotor outcomes up to 27 weeks post-injury (wpi) and anatomical repair at 29 wpi; which is longer than any previous chronic transplantation study. The goal of this experiment was to provide proof-of-principle for the potential of SKP-SCs (without co-treatments) to promote repair and functional recovery in the chronic SCI setting. We report that SKP-SCs survived long-term at the site of chronic SCI, integrated into the host spinal cord and mitigated astroglial scar formation, promoted axonal growth and ensheathment/myelination, and stimulated a massive increase in the presence of endogenous SCs. Importantly, SKP-SC transplantation elicited better functional outcomes and improved bladder pathology.

RESULTS

Transplanted SKP-SCs Survive and Bridge the Chronic SCI Lesion

The experimental timeline is summarized in Figure 1A. GFP+ neonatal SKP-SCs were prepared for transplantation and 98.4% of the labeled cells were SCs as demonstrated by colocalization with S100β. Rats received either a neonatal SKP-SC transplantation or a medium injection at 8 weeks post-SCI, underwent regular behavioral tests throughout the study, and were perfused at 21 weeks post-transplant or 29 weeks post-SCI. The time of transplant (TofT) control group was perfused at 8 weeks post-SCI to assess the injury site at the time of treatment. Eight weeks after SCI in the TofT control group, the lesion site was prominent, and filled with residual tissue (much of which is IBA1+) and GFAP+ tissue strands indicative of reactive astrocytes (Figure 1B). Importantly, we observe variability from animal to animal in the cavity size, lesion size, existing substrate, and extent of debris at injury epicenter at the time point at which the cells would have been transplanted. At 29 wpi, lesion sites in cell culture medium-injected rats displayed large empty cavities that were walled off by a sharp border of GFAP+ astrocytes (Figure 1C). In contrast, in animals that received SKP-SCs, the lesion site was spanned by bridges of GFP+ cells (Figure 1D). In sections immunostained for GFP to enhance visibility (e.g., Figure 1E) and with nuclear staining, GFP+ cells were present in the spinal cord in all animals, although there was a high degree of variability in cell numbers. Eight of 15 animals that received SKP-SCs contained 70–120,000 GFP+ cells, whereas four animals had 20–70,000 cells, and three rats had fewer than 20,000 cells left in their spinal cords at 21 weeks post-transplantation (Figure 1F). The majority of the SKP-SCs displayed predominant rostro-caudal orientation deviating (on average) not more than 25°–30° from the rostro-caudal axis of the spinal cord and immunostaining for KI67 indicated minimal proliferation (<0.1%) of the transplanted cells (Figure S1).

SKP-SC Transplantation Increases Intact-Appearing Tissue around the Chronic Injury Site

We defined the lesion site as tissue with absent or disrupted cytoarchitecture as revealed by GFAP-immunostaining of the host astrocytes. Hence, the lesion volume measures the destroyed and/or grossly abnormal spinal cord tissue, including the cavity volume. We saw no differences in lesion volume across the groups (Figure 1G). To assess the amount of intact-appearing tissue surrounding the SCI site, we measured residual GFAP+ spinal cord tissue with intact-appearing cytoarchitecture in the spared rim as well as within the lesion. At 29 wpi, both SKP-SC- and medium-treated animals had significantly more intact-appearing tissue at the lesion epicenter than TofT controls (Figure 1H), indicating an expansion of intact-appearing tissue between 8 and 29 wpi. The amount of intact-appearing tissue was significantly different between the SKP-SC- and medium-treated animals only when high survival of transplanted SKP-SCs was observed (Figure S2; Supplemental Experimental Procedures).

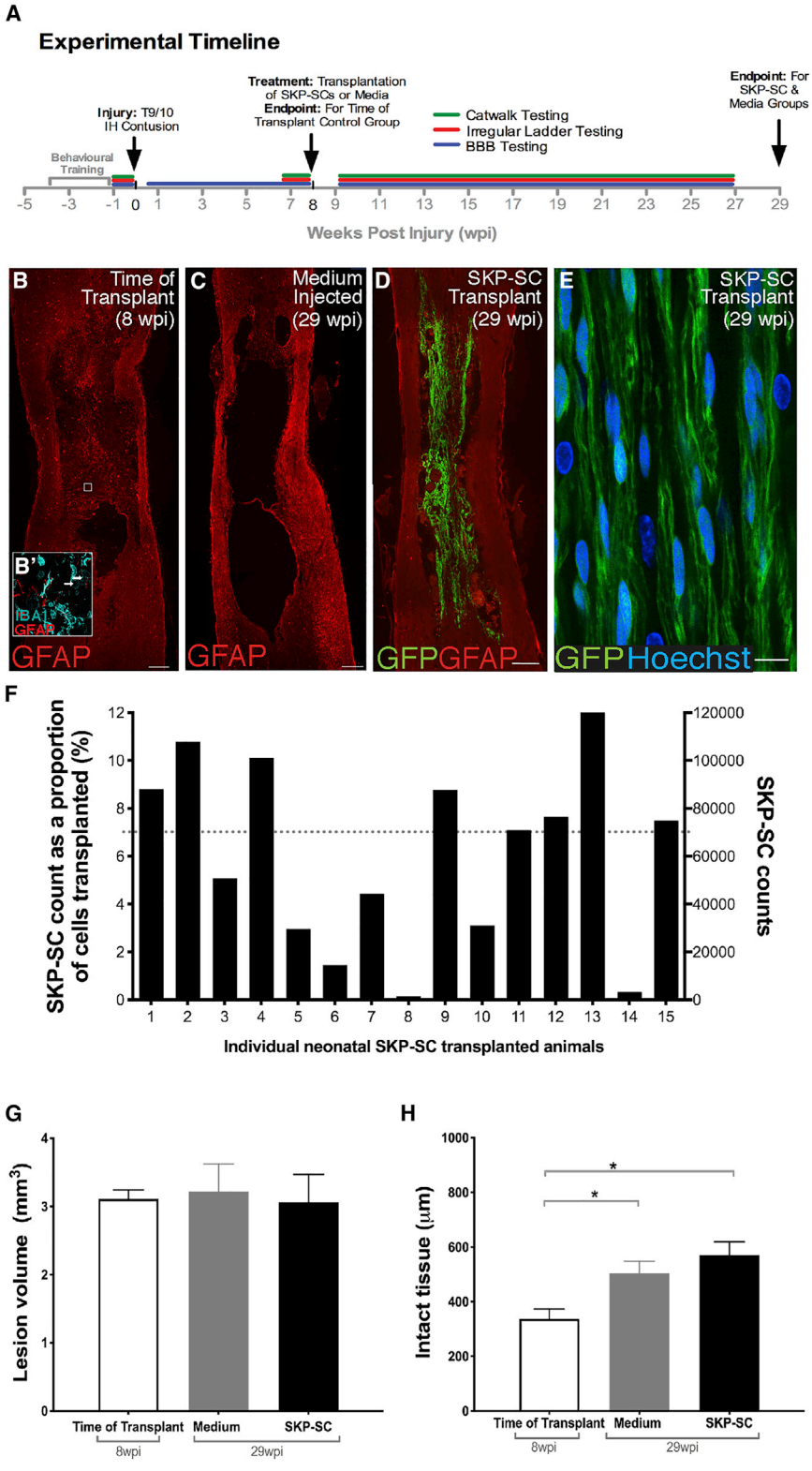

Figure 1. SKP-SC Grafts Survive *In Vivo* in the Chronically Injured Spinal Cord

(A) Experimental timeline.

(B–D) Photomicrographs of GFAP-immunostained contused spinal cords from a TofT control animal (B), a medium-injected control animal (C), and a SKP-SC transplanted animal (D). (B) At 8 wpi, the lesion is filled with both IBA1+ macrophages/microglia (teal in B′, arrows) and some residual GFAP+ (red in B and B′) host tissue. (C) By 29 wpi, the representative medium control spinal cord has developed a large fluid-filled cavity. (D) SKP-SCs (GFP+) integrate into the lesion sites and bridge the cavity.

(E) High-magnification image of GFP+ SKP-SCs.

(F) SKP-SC counts at 29 wpi for all transplanted rats. Dotted line represents the 70,000-cell level.

(G) The mean lesion volume was similar among the three main groups.

(H) Mean thickness of intact-appearing GFAP+ tissue per group. Note that the TofT control group (8 wpi) had significantly less intact-appearing tissue than the medium (*p = 0.028) and SKP-SC (*p = 0.003) groups (29 wpi). See also Figures S1 and S2.

In (G) and (H): SKP-SC, n = 15; medium, n = 13; TofT, n = 8. Data represented as mean ± SEM. ANOVA with least significant difference (LSD) post-hoc test in (G) and (H). Scale bars: 200 μm in (B)–(D), 20 μm in (B′), and 10 μm in (E).

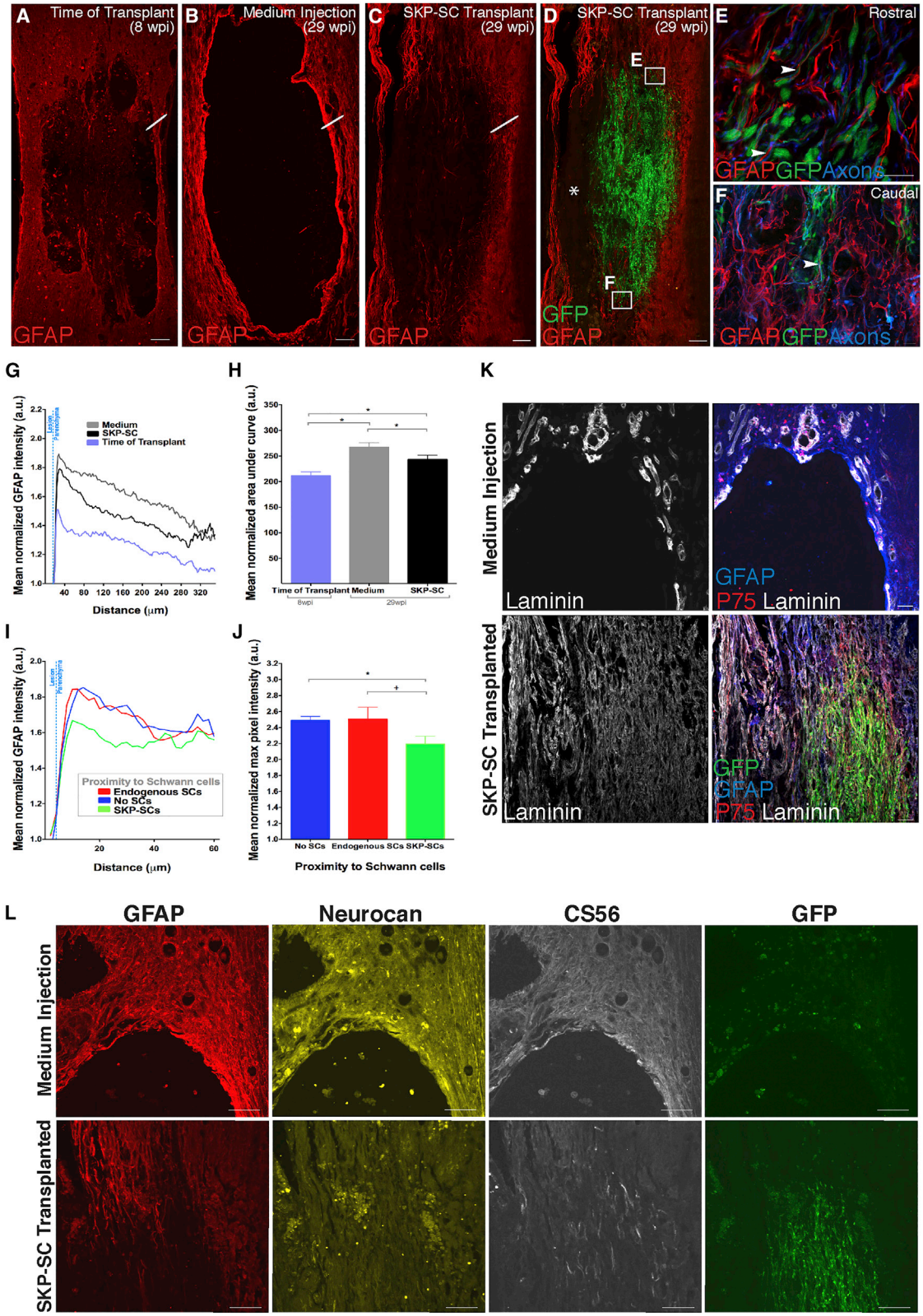

(legend on next page)

SKP-SCs Integrate into Spinal Cord Tissue, Mitigate the Formation of the Glial Scar, and Provide a Permissive Substrate for Axon Growth

A major contributor to regeneration failure after SCI is the glial and fibroblastic scar (Dias et al., 2018; Filous and Silver, 2016), although certain aspects of these cellular responses can be beneficial (Anderson et al., 2016). At 8 wpi, a loose mesh of astrocytic processes bordered and extended into the site of SCI, and the lesions were commonly filled with phagocytic cells and residual tissue septae (Figure 2A). By 29 wpi, in the medium control group, most residual tissue had cleared, and the lesions were characterized by "empty" cavities, presumably fluid-filled *in vivo*, with sharply demarcated borders exhibiting increased GFAP expression (Figures 2B, 2K, and 2L). In contrast, at 29 wpi in the SKP-SC group, host astrocytes extended multiple fine processes into the SKP-SC transplant, particularly at the rostro-caudal boundaries of the lesion site (Figures 2C–2F, 2K, and 2L).

Densitometric analysis (along the white line spanning the cavity-parenchyma interface in Figures 2A–2C) revealed significantly higher GFAP expression in both 29 wpi groups compared with the TofT control group, indicating that reactive gliosis increases over time after SCI (Figures 2G and 2H). Progressive gliosis was mitigated in SKP-SC-treated animals; GFAP expression was reduced compared with medium-only controls (Figures 2G and 2H). In SKP-SC-treated rats, GFAP intensity was high adjacent to regions of cavitation and close to endogenous SCs, and reduced in astrocytes neighboring SKP-SCs (Figure 2I; quantified in Figure 2J). These effects of SKP-SCs delivered in chronic SCI are similar to our observations following sub-acute transplantation (Biernaskie et al., 2007).

SKP-SCs also provided a more permissive growth substrate. In medium-treated controls, laminin, which is expressed by SCs in peripheral nerves, was typically restricted to blood vessels in the spinal cord and to the host SCs present in the spared tissue margin of the lesion site (Figure 2K, top row). In contrast, in SKP-SC-treated animals, the spinal cord tissue displayed extensive laminin immunoreactivity. Laminin was expressed both within the transplants and in the host tissue bordering the SKP-SC bridges where many of the laminin+ cells were GFP− endogenous SCs expressing P75NTR (Figure 2K, bottom row).

Integration of SKP-SCs and reduced GFAP immunoreactivity led us to ask whether these differences reflected a change in the inhibitory nature of the glial scar. Inhibitory proteins associated with the glial scar, including neurocan and chondroitin sulfate proteoglycan (CSPG) (CS56 labeling), were expressed in a sharply demarcated boundary around lesion cavities in the medium controls (Figure 2L, top row), but not at the interface of SKP-SC grafts and host tissue (Figure 2L, bottom row) suggestive of a difference in CSPG expression and good integration.

SKP-SCs Promote Growth/Regeneration of Host Axons

To determine whether SKP-SC transplantation enhances axon growth, we first examined spinal cord sections immuno-labeled with antibodies against large- and

Figure 2. SKP-SCs Mitigate the Formation of the Chronic Glial Scar

(A–C) Photomicrographs showing the differences in astrocyte organization and reactivity in the (A) TofT, (B) medium-injected, and (C) SKP-SC groups.

(D) Same as (3C) together with the GFP+ SKP-SCs (green). Note that * denotes area filled with endogenous myelinating and non-myelinating SCs (SC markers not shown in image).

(E and F) Insets of astrocyte processes overlapping in close proximity with SKP-SCs (arrowheads) at the rostral (E) and caudal (F) host-graft interfaces in (D).

(G) Average GFAP (astrocyte) intensity traces depicted as line drawn in (A)–(C) representing the transition from the lesion to the host parenchyma for the three groups.

(H) Bar graphs representing the mean area under the curve for the waveforms shown in (G). Note the lower GFAP immunoreactivity in the TofT group versus medium (*$p < 0.001$) and SKP-SC (*$p = 0.019$) groups, and in the SKP-SC group versus medium group (*$p = 0.030$).

(I) GFAP intensity traces in proximity to SKP-SCs, endogenous SCs, or no-SCs (cavity) in SKP-SC transplanted spinal cords.

(J) Bar graphs representing the mean normalized maximum GFAP pixel intensity in each line used to generate the waveforms shown in (I). Note the lower GFAP intensity in locations next to SKP-SCs compared with areas next to the cavity (no-SCs; *$p = 0.01$) or next to endogenous SCs (trending toward significance; +$p = 0.051$).

(K) Photomicrographs of laminin immunoreactivity at the rostral lesion-host spinal cord interface at 29 wpi. In the medium-treated group, laminin immunoreactivity is largely associated with blood vessels whereas in the SKP-SC transplanted group laminin is widely expressed throughout the graft site containing SKP-SCs and in the surrounding parenchyma.

(L) Lesion-host spinal cord interface at 29 wpi in the SKP-SC and medium groups, immunolabeled for GFAP, neurocan, the pan-CSPG marker CS56, and GFP of the same region of interest; note the minimal glial scar formation with very little CSPG expression in the SKP-SC transplanted spinal cord. In (G)–(J): SKP-SC, $n = 15$; medium, $n = 15$; TofT, $n = 8$. Data represented as mean ± SEM in (H) and (J). ANOVA with LSD post-hoc test in (H) and repeated measures ANOVA with paired t tests in (J). Scale bars: 200 μm in (A)–(D), 20 μm in (E) and (F), 100 μm in (K), and 50 μm in (L).

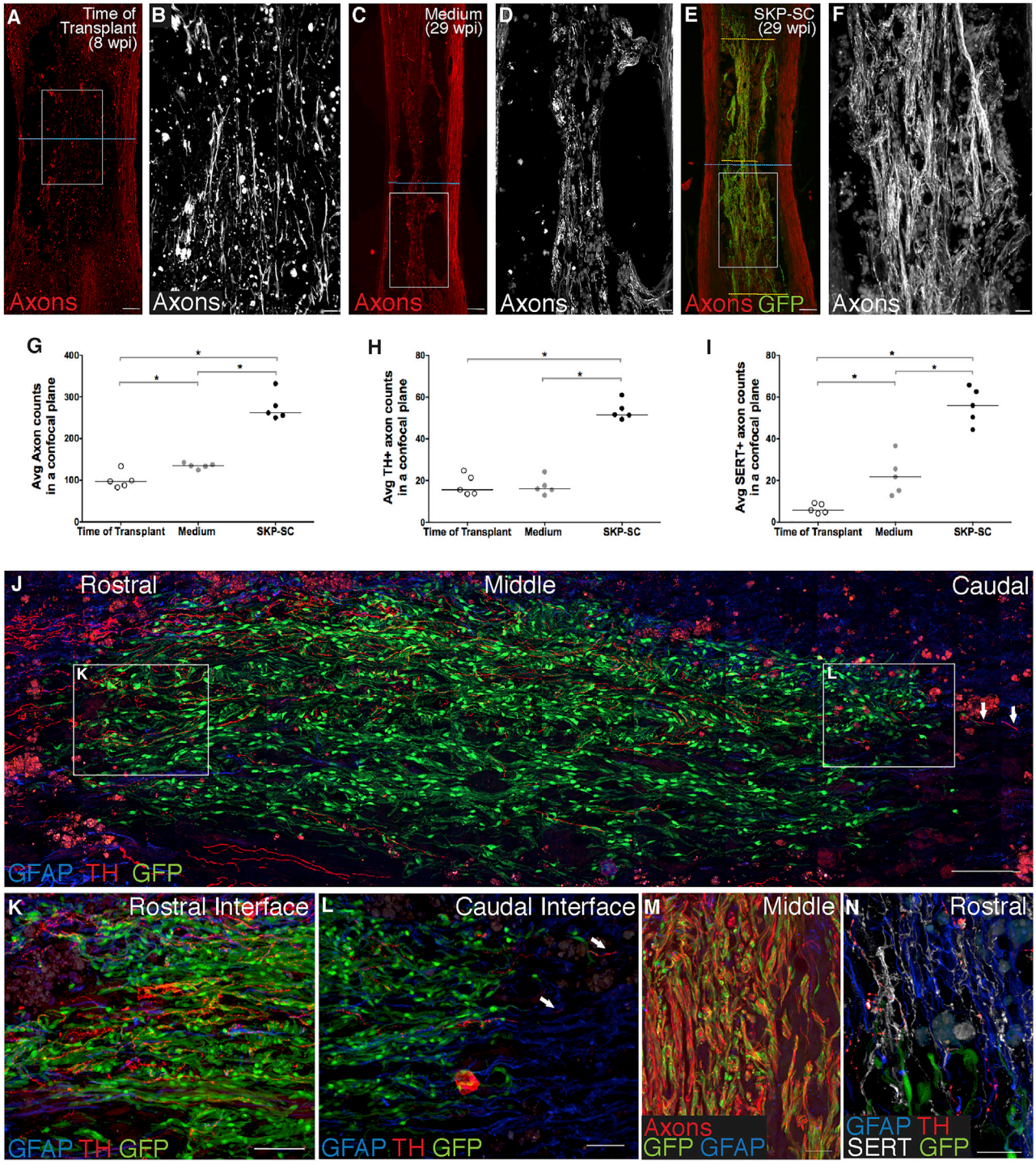

Figure 3. SKP-SCs Promote Axonal Growth/Regeneration into the Chronic Lesion

(A–F) Representative photomicrographs of axons (NF-200/βIII-tubulin) at low (A, C, and E; red) and high (B, D, and F; boxed regions from A, C, and E; white) magnification for the TofT (8 wpi; A and B), medium (29 wpi; C and D), and SKP-SC (29 wpi;E and F) groups. Blue dotted blue lines in (A), (C), and (E) represent the narrowest point through the lesion where axon counts were conducted shown in (G)–(I); yellow dashed lines in (E) indicate the regions used for axon counts in the rostral, middle, and caudal region of the lesion (Figures S3F–S3I). (G–I) Average NF-200/βIII-tubulin+ (G), TH+ (H), and SERT+ (I) axon numbers were counted in animals with high graft survival (above the gray line in Figure 1F) within a single confocal plane and compared with controls. (G) Note more than twice as many NF-200/βIII-tubulin+

(legend continued on next page)

small-caliber axons (NF-200/βIII-tubulin) in animals with high cell survival (above the gray line in Figure 1F). At 8 wpi, some spared host tissue bridged the lesion site and contained small bundles of axons running in a rostro-caudal orientation (Figures 3A and 3B). By 29 wpi, lesions in medium-treated controls were characterized by tightly demarcated cavities with only rare host tissue septae still containing some axons (Figures 3C and 3D). In contrast, SKP-SC-treated rats with high numbers of surviving SKP-SCs contained many axons extending through SKP-SC bridges, most of which also maintained a rostro-caudal orientation (Figures 3E, 3F, and 3M). The average number of axons within a single confocal plane at the lesion epicenter of the spinal cord (counted along the blue stippled line in Figures 3A, 3C, and 3E; i.e., with the spared rim included) was less than 140 in medium control animals at 29 wpi. There were twice as many axons present after SKP-SC transplantation, mostly in the cell bridges crossing the lesion (Figure 3G).

When we examined specific populations of TH+ and SERT+ axons, more were found at the lesion site in the SKP-SC-treated animals compared with both control groups (Figures 3H–3L, and 3N). Predictably, there were more TH+ and SERT+ axons at the rostral and middle levels of the SKP-SC bridges than the caudal level (counted at the yellow lines shown in Figure 3E), reflecting their origin from the brainstem (Figure S3). Numerous SERT+ and TH+ axons had advanced to the caudal host interface and a small number crossed this interface and entered the caudal spinal cord where they appeared to stop within several hundred microns (Figures 3J and 3L). The tortuous appearance of those axons, taken together with the rostro-caudal gradient in their density, suggests that these monaminergic axons had grown through the SKP-SC bridges but we cannot know for certain whether the axons exited the grafts in the absence of tract tracing. There were no differences in the total number of axons (NF-200/βIII-tubulin) or CGRP+ axons across these rostro-caudal levels (Figure S3). Of note, peptidergic sensory axons expressing substance P or CGRP represented <3% of all the axons in these grafts (Figure S3).

SKP-SCs Myelinate Axons in the Chronically Injured Spinal Cord

To determine whether transplanted SKP-SCs myelinated axons, we performed triple labeling for GFP, P0, and axons (NF-200/βIII-tubulin; Figures 4A–4C). We found clear evidence of ensheathment/myelination by SKP-SCs. At 29 wpi, 73% of the SKP-SCs were myelinating, as defined by the formation of a thin GFP+ cytoplasmic layer surrounding P0+ myelin ensheathing a NF-200+ or βIII-tubulin+ axon. Ensheathment/myelination was further confirmed by immuno-labeling for KV1.2 (Figures 4D and 4E), the main potassium channel in the juxtaparanodal axon membrane and CASPR (Figures 4F and 4G), which contributes to the septate junctions between the axon and the paranodal loops of myelin-forming SCs. SKP-SCs and endogenous SCs were generally found in areas with abnormal or absent astrocyte cytoarchitecture, which tended to be devoid of oligodendrocyte myelin. About half (52%) of the axons that had grown into the SKP-SC bridges were wrapped in P0+ myelin.

SKP-SC Transplantation Augments Spontaneous Repair by Endogenous SCs

In our previous studies (Biernaskie et al., 2007; Sparling et al., 2015), SKP-SC transplantation prompted an increase in endogenous myelinating SCs occupying the spinal cord. This potential repair mechanism is of interest considering recent work suggesting that centrally derived platelet-derived growth factor receptor alpha+ (PDGFRα) oligodendrocyte precursor cells (OPCs) give rise to SCs after demyelination (Zawadzka et al., 2010) and contusion SCI (Assinck et al., 2017b). To address the endogenous SC response in this study, we examined spinal cord sections for GFP− (i.e., host) myelinating (P0+) and non-myelinating (P75NTR+) SCs.

axons in the SKP-SC group compared with the medium (*p = 0.008) or TofT groups (*p = 0.008), and significantly more axons in the medium versus the TofT group (*p = 0.032). (H) More TH+ axons were counted in the SKP-SC group compared with the medium (*p = 0.008) and TofT groups (*p = 0.008). (I) There were also significantly more SERT+ axons running through the narrowest part of the cord in the SKP-SC group compared with the medium (*p = 0.008) and TofT groups (*p = 0.008), and more SERT+ axons in the medium group compared with the TofT group (*p = 0.008).

(J–L) Photomicrographs of TH+ axon (red) growth through the SKP-SC grafted lesions at 29 wpi. (K and L) A large number of descending TH+ axons enter the graft (J and K) and a small number of those axons leave the caudal end of same graft and re-enter the host (arrows, J and L).

(M) Representative photomicrograph demonstrating the large number of axons within the SKP-SC graft at 29 wpi.

(N) Representative photomicrograph showing TH+ axons and SERT+ axons near the rostral host-graph interface. In (G)–(I): SKP-SC, n = 5; medium, n = 5; TofT, n = 5; see Supplemental Experimental Procedures. Individual data points for each animal are presented with group medians indicated by solid black lines in (G)–(I). Kruskal-Wallis with Mann-Whitney U test (MWU) in (G), (H), and (I). Supplemental Experimental Procedures Scale bars: 200 μm in (A), (C), and (E), 100 μm in (J), 50 μm in (B), (D), (F), (K), and (L), and 20 μm in (M) and (N).

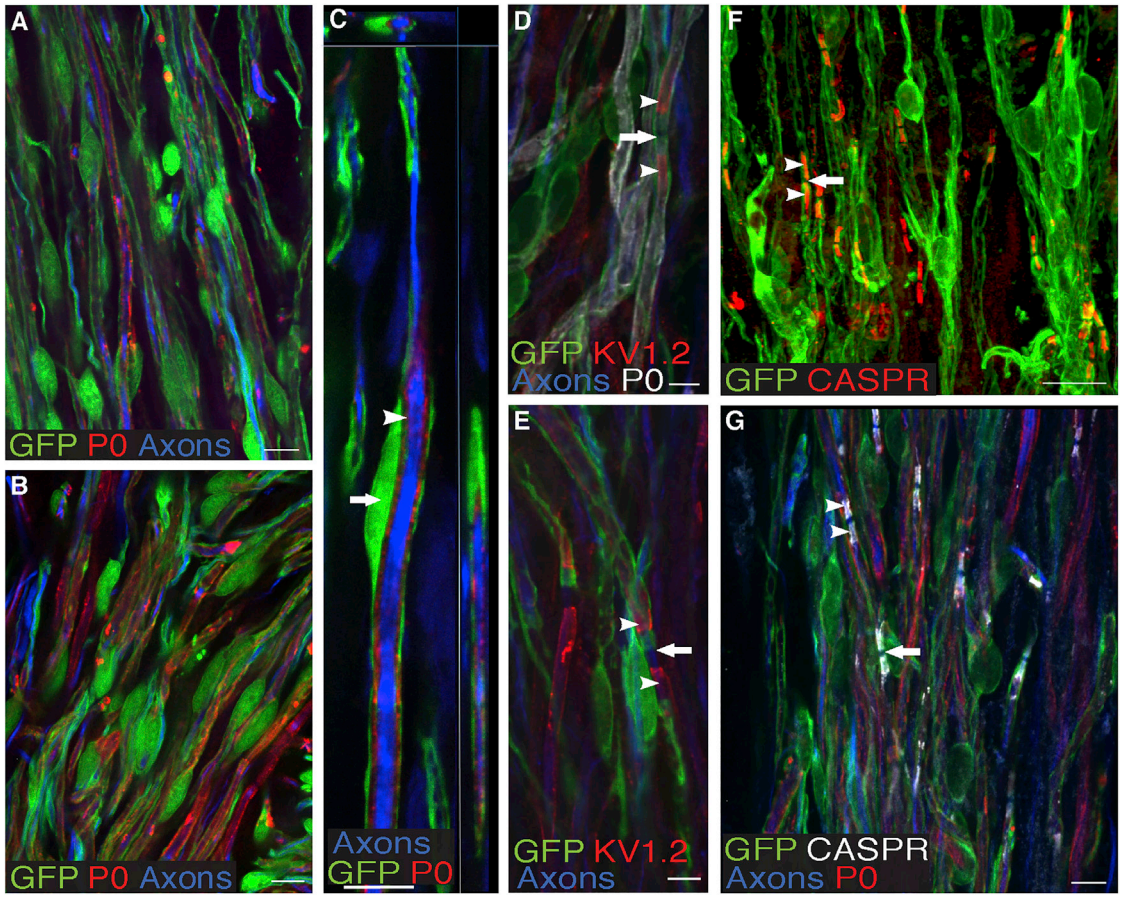

Figure 4. SKP-SCs Myelinate Axons

(A–C) Close-up micrograph of an SKP-SC bridge demonstrating the formation of SC myelin (P0, red) around host axons (combined NF-200 and βIII-tubulin, blue) by GFP+ SKP-SCs (green). (C) Note the cell body of the SKP-SC (arrow) and the layers of P0 (arrowhead) sandwiched between the axon and the GFP+ cytoplasm in the outer layer of the SKP-SC.

(D–G) Photomicrographs of axons ensheathed by GFP+ SKP-SCs and immunostained for KV1.2+ potassium channels (D and E) and CASPR (red in F and white in G). Note that SKP-SC-ensheathed axons showed appropriate nodal structures, including nodes of Ranvier (arrows, D–G) with ribbon-like labeling of the paranode by CASPR (arrowheads, F and G) and the juxtaparanode by KV1.2 (arrowheads, D and E) on either side of the node. Scale bars: 20 μm in (A), (B), and (G), 10 μm in (C) and (F), and 5 μm in (D) and (E).

P0+ SC myelin was often encountered in the lesion walls and the residual tissue strands in and around the lesions in the TofT (Figure 5A) and medium (Figures 5B and 5F) control groups. However, more P0+ myelin sheaths were found in animals that received SKP-SCs (Figures 5C–5D and 5G). In SKP-SC-treated animals, myelin sheaths were SKP-SC-derived (P0+, GFP+) or host SC-derived (P0+, GFP−); there were more host SC-derived myelin sheaths in SKP-SC-treated animals, even when SKP-SC survival was limited (Figure 5D). There was no correlation between the GFP+ volume and the total P0+ volume ($r = 0.030$, $p = 0.916$) in the SKP-SC-treated group. Importantly, this suggests that even the transient presence of SKP-SCs within the injured spinal cord enhanced the endogenous SC response. GFP+ SKP-SCs accounted for a relatively small proportion of the P0 myelin by volume, as only 9.6% of the overall P0 volume in animals that received SKP-SCs overlapped with GFP+ cells (green portion of bar in Figure 5I). Hence, endogenous SCs generated the clear majority of P0 myelin found 29 weeks after SKP-SC transplantation (black portion of bar in Figure 5I).

We also analyzed the location of SC-derived myelin at the level of injury in all groups and found that both the TofT and medium control groups had more endogenous SC myelin in the spared tissue than in the lesion site (Figure 5J). In contrast, the SKP-SC group exhibited similar amounts of SC myelin in both locations. SKP-SC-treated animals showed a larger P0 volume inside the lesion site than either control group, and a larger P0 volume outside the lesion compared with the TofT control group only

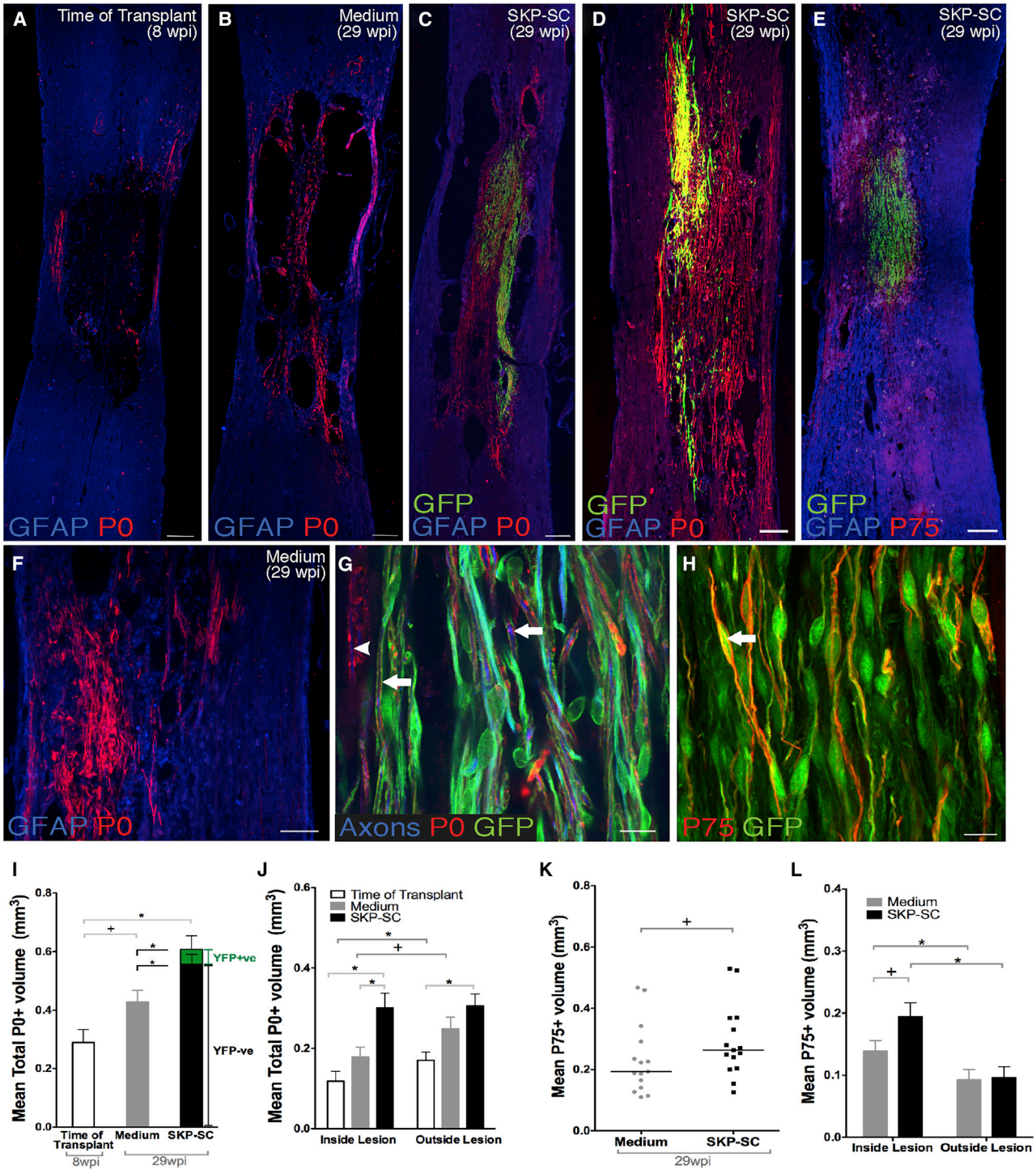

Figure 5. The SKP-SC Group Contains Significantly More SC Myelin and Non-myelinating SCs

(A–D) Overview micrographs of the spinal cords from the TofT (A), medium-injected (B), and the GFP+ SKP-SC transplanted (C) group immunostained for P0, GFAP, and GFP. (C and D) Note the extensive presence of P0+/GFP− myelin produced by endogenous SCs in the spinal cord of animals with both high (C) (>70,000 SKP-SCs at 29 wpi) or low (D) (<50,000 SKP-SCs at 29 wpi) survival of transplanted SKP-SCs.

(E) Abundant presence of endogenous non-myelinating SCs expressing P75NTR (labelled as P75) in the absence of GFP, often observed in close proximity to GFP+ SKP-SC grafts.

(legend continued on next page)

(Figure 5J). Interestingly, the amount of intact-appearing tissue positively correlated with overall P0 volume ($r = 0.502$, $p < 0.001$), P0 volume inside the lesion ($r = 0.429$, $p = 0.009$), and P0 volume outside the lesion ($r = 0.557$, $p < 0.001$), suggesting that sparing or survival of host tissue is associated with greater SC myelin content in the injured spinal cord.

P75NTR is highly expressed in non-myelinating SCs and we found bright P75NTR+ cells with the characteristic spindle-shaped morphology of non-myelinating SCs in the spared host tissue of all groups (Figures 5E and 5H). In SKP-SC-transplanted rats, most of the P75NTR+ cells in the tissue rim were GFP− endogenous SCs, whereas those in the lesion bridges were often GFP+ transplanted cells (Figure 5H). Approximately 9% of the total P75NTR+ volume was GFP+. Quantitative examination of P75NTR expression bore results like those for P0; the P75NTR volume correlated with the amount of intact-appearing tissue ($r = 0.388$, $p = 0.042$), suggesting that increased intact-appearing host tissue is associated with enhanced SC content in general, not just increased SC ensheathment/myelination.

Transplantation of SKP-SCs 8 wpi Results in Better Locomotor Outcomes

Having established that SKP-SC transplants promote histological repair in chronic SCI, we asked whether these cells also enhanced functional locomotor recovery. The BBB (Basso, Beattie, and Bresnahan) scores in both groups showed spontaneous locomotor recovery from the time of contusion SCI to the TofT (8 wpi), and no functional decline was observed in the weeks after SKP-SC transplantation or medium injection. A repeated measures ANOVA indicated that the difference between the medium and SKP-SC groups changed over the last 16 weeks of the study with a significant group difference at weeks 19 and 21 (Figure 6A). The amount of P0 expression outside the lesion correlated with the BBB scores at 27 wpi ($r = 0.648$, $p = 0.009$).

To complement the open field measurements, we performed Catwalk gait analysis. Average forelimb stride length was ~140 mm pre-injury, dropped to 100 mm post-injury, and remained at that value in the medium group at 26 wpi. In contrast, in rats receiving SKP-SC, stride length recovered partially to 108 mm at 26 wpi. Repeated measures ANOVA revealed that the difference between the medium and SKP-SC groups changed for both forelimb and hindlimb stride length (normalized to each animal's pre-treatment values) over the last 16 weeks of the study with a significant group difference indicated at each time point denoted with an asterisk (Figures 6B and 6C). Thus, the SKP-SC group maintained longer forelimb and hindlimb stride lengths compared with the medium-only group, which showed a further decline in the hindlimbs (Figure 6C). The injury itself affects hindlimb motor and sensory function but a decrease in hindlimb stride length results in a compensatory decrease in forelimb stride length (Figure 6B). SKP-SC treatment also resulted in a reduced angle of hindlimb paw rotation and a decreased frequency of abnormal gait patterns compared with the medium-only group (Figure S4). No significant differences were detected on hindlimb print width or intensity parameters, the BBB subscore, or the horizontal ladder analysis (Figure S4).

SKP-SC Transplantation Reduces Bladder Pathology Observed after SCI

Autonomic dysfunction is a major concern after SCI and improving bladder function has been ranked a high priority among people living with SCI (Anderson, 2004).

(F) Note the presence of P0+ myelin generated by endogenous (GFP−) SCs in a medium-injected spinal cord.
(G) High-magnification photomicrograph of axons (NF-200/βIII-tubulin) ensheathed by either GFP+ SKP-SCs (arrow) or GFP− endogenous SCs (arrowhead).
(H) Non-myelinating P75NTR+ SCs derived from transplanted GFP+ SKP-SCs (arrow) within the lesioned spinal cord at 29 wpi.
(I) Quantification of P0+ volumes by treatment groups; the green segment denotes the mean volume of P0+/GFP+ SKP-SCs. The SKP-SC group had significantly greater SC myelin volume (black and green bar combined) than both the medium (*$p = 0.005$) and the TofT control (*$p < 0.001$) groups. Importantly, the mean volume of P0+/GFP− endogenous SCs was higher in the SKP-SC group (black portion of bar) than in the medium group (gray bar; *$p = 0.038$). There was no difference observed between the TofT control and medium control groups (trending toward significance; +$p = 0.068$).
(J) Distribution of P0+ myelin inside the lesion versus outside the lesion, i.e., in the spared host rim. P0+ volume in the SKP-SC group was greater than the TofT control group both inside (*$p = 0.001$) and outside (*$p = 0.006$) of the lesion, and greater than the medium group inside the lesion (*$p = 0.005$). The TofT control group showed significantly greater P0+ volumes outside the lesion as compared with inside (*$p = 0.002$); the medium group showed no difference (trending toward significance; +$p = 0.067$).
(K) The SKP-SC group trended toward larger p75NTR+ volumes versus the medium group (+$p = 0.074$).
(L) Both the SKP-SC and medium groups showed significantly greater P75NTR+ volume inside the lesion compared with outside (*$p = 0.002$ and *$p = 0.014$, respectively); the SKP-SC group approached statistical significance toward a higher p75NTR+ volume versus the medium group inside the lesion only (+$p = 0.057$). In (I)–(L): SKP-SC, $n = 15$; medium, $n = 15$; TofT, $n = 8$. Individual data points for each animal presented with group medians indicated by solid black lines in (K) and data presented as means ± SEM in (I), (J), and (L). ANOVA with LSD post-hoc test in (I) and (J), paired t test in (J) and (L), MWU in (K), and t test in (L). Scale bars: 200 μm in (A)–(F) and 10 μm in (G) and (H).

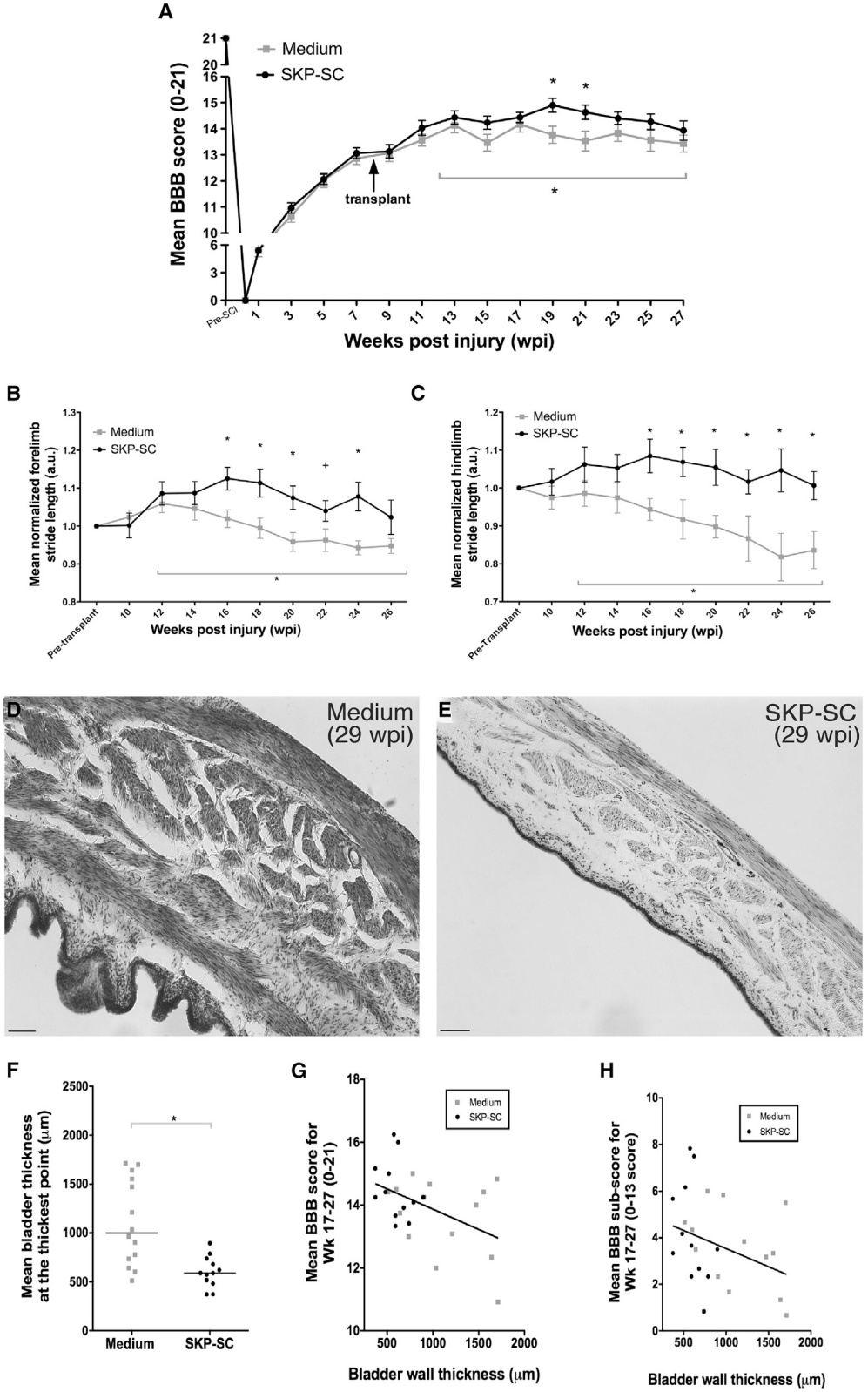

(legend on next page)

Although all rats regained spontaneous micturition weeks after injury, ongoing bladder deficits do persist. We can speculate that the T9/T10 contusion injury may damage supraspinal tracts for bladder control and/or a subset of the sympathetic neurons that originate from the spinal cord. We conducted post-hoc histological analysis of the bladder wall to examine the effects of SKP-SC transplantation on bladder pathology. Qualitative examination revealed bladder wall "thickenings" in the medium-treated animals (Figure 6D) that were absent in animals transplanted with SKP-SCs (Figure 6E). Measurements of the thickest point revealed that bladder walls of medium-treated rats were almost twice as thick as SKP-SC-treated rats (Figure 6F). These bladder wall thickenings are typical of bladder-sphincter dyssynergia and/or a lack of inhibitory supraspinal input causing detrusor over-activity (de Groat et al., 1990), suggesting that these issues play less of a role after SKP-SC transplantation. The bladder wall thickness was negatively correlated with both BBB and BBB subscore (Spearman's rho = −0.414 and −0.425, p = 0.036 and 0.030, respectively, Figures 6G and 6H). For a full list of relevant correlations, see Table S2.

DISCUSSION

SKP-SCs transplanted 8 weeks after a thoracic spinal cord contusion survive for more than 5 months at the site of chronic SCI, integrate with spared host tissue, and promote several types of neural repair, including axonal growth/regeneration and SC ensheathment/myelination. Endogenous SCs exhibited a substantial reparative response, which was enhanced by transplanted SKP-SCs. Importantly, SKP-SC transplantation at chronic stages of SCI spurred the growth/regeneration of supraspinal axons into and through the bridges of grafted cells, improved locomotor function, and reduced bladder pathology. The translational relevance of this study is strengthened by our experimental approaches which include (1) the use of a clinically relevant contusion model; (2) the use of a delay in intervention (8 wpi; chronic transplantation), which provides a reasonable time frame for translation with regards to optimal clinical trial design; and (3) the decision to follow the animals for more than 5 months after intervention allowing us to define ongoing histological and behavioral changes. Together, our findings suggest that SKP-SCs represent a promising intervention for SCI, with the potential to confer benefits in the chronic setting.

Our estimates indicate that up to 12% of the transplanted SKP-SCs survived in the host spinal cord for 21 weeks post-transplantation. However, this likely represents an underestimate, as we did not account for cells lost during the transplantation process, which may have been ∼20% according to previous findings (Hill et al., 2006). The extensive integration of SKP-SCs observed at the endpoint was unexpected and prompted us to analyze the injury site at 8 wpi in the TofT control group to better understand the environment encountered by the transplanted cells.

At 8 wpi the lesion was full of mononuclear cells (many of which were IBA1+), lacked a dense glial scar, and contained numerous GFAP+ processes as well as small bundles of axons that ran rostro-caudal through the site of injury on either side of the ventral fissure. We observed considerable variability in lesion size, cavity size, and the amount of

Figure 6. Transplantation of SKP-SCs after Chronic SCI Improves Locomotor Outcomes and Bladder Wall Pathology

(A) SKP-SC transplanted animals reached higher mean open field locomotion (BBB) scores than the medium-injected controls. A repeated measures ANOVA examining weeks 12–27 showed a significant interaction (*p = 0.032), indicating that the difference between those two groups changed over time during that period. Follow-up testing revealed significantly higher BBB scores in the SKP-SC group at weeks 19 (*p = 0.012; t test) and 21 (*p = 0.026; t test).

(B and C) A repeated measures ANOVA of CatWalk footprint analysis over the last 16 weeks yielded a significant interaction in normalized forelimb (*p = 0.046; B) and hindlimb stride length (*p = 0.032; C). (B) Normalized forelimb stride length was significantly greater for SKP-SC-treated animals (compared with medium control) at 16, 18, 20, and 24 wpi (p < 0.013; t test) and showed a trend toward significance at 22 wpi (+p = 0.069; t test). (C) Normalized hindlimb stride length showed significant differences at every time point between 16 and 26 wpi (*p < 0.039).

(D and E) Representative (near-median values) photomicrographs of bladder wall stained with cresyl violet from the medium control group (D) and the SKP-SC transplanted group (E).

(F) Quantification of average bladder wall thickness at the thickest point yielded that the SKP-SC group had significantly thinner bladder walls than the medium-treated group (*p = 0.001; MWU).

(G and H) Scatterplots of bladder wall thickness at the thickest point versus average BBB score (G) or average BBB subscore (H) from week 17 to 27 for both medium (gray squares) and SKP-SC (black dots) groups. Bladder wall thickness showed a significant negative correlation to both BBB and BBB subscore (Spearman's rho = −0.414 and −0.425, p = 0.036 and 0.030, respectively), i.e., animals with better locomotor function also had thinner bladder walls. See also Figure S4 for further behavioral outcomes. In (A)–(C): SKP-SC, n = 15; medium n = 15 and in (F)–(H): SKP-SC, n = 12; medium, n = 14. Data presented as group means ± SEM in (A)–(C) and individual data points for each animal are presented with group medians indicated by solid black lines in (F) and the line of best fit indicated by the solid black lines in (G) and (H). Scale bars, 100 μm in (D) and (E).

existing substrate in the TofT control group. The substantial number of rostro-caudal oriented spared axons, together with astrocytic processes, may have provided a suitable substrate for SKP-SCs and endogenous SCs in this study aiding to bridge the lesion sites.

Axons are known to grow into and within nerve-derived SC grafts, but they tend to struggle to leave those grafts and grow back into the astrocyte-rich host parenchyma also known as "off-ramp" problem (Wiliams and Bunge, 2012). Despite the disruption of normal GFAP cytoarchitecture at the lesion site, SKP-SC and astrocyte processes often intermingled at the transplant-host interface and it was noted that SKP-SCs trended towards inducing less GFAP expression in adjacent astrocytes than endogenous SCs near the injury site. This arrangement appeared to provide a permissive growth environment for axons entering and exiting the grafts. Importantly, such permissive SC graft/spinal cord interfaces have only been observed previously for nerve-derived SC transplants combined with Matrigel (Williams et al., 2015) or engineered to overexpress GDNF (Deng et al., 2013). Of the thousands of axons found in SKP-SC bridges, ~40% were of brainstem origin (based on immunolabeling for TH and SERT). The presence of TH+ axons at the caudal transplant-host interface was surprising, considering that the growth/regeneration of supraspinal axons in response to nerve-derived SCs typically requires the addition of co-treatments (i.e., other cells, drugs, biomaterials, or trophic support; for review see Assinck et al., 2017a; Bunge, 2016; Tetzlaff et al., 2011). While this may reflect an advantage of SKP-SCs over nerve-derived SCs, it is important to note that, in the absence of tract tracing, the exiting and connectivity of those TH+ axons, and thus their contribution to functional recovery, remained uncertain in this study.

The increase in intact-appearing rim tissue between 8 and 29 wpi was unexpected and may be due in part to the release of a second wave of injury-related factors (e.g., cytokines) triggered by the transplantation surgery or increases in spinal cord area associated with growth. Given the state of the lesion site at 8 wpi, it remains unclear whether the thickening of the rim over time was the result of neuroprotective or reparative mechanisms, as the sparing and remyelination of denuded axons and the growth and myelination of new axons may both have contributed. Resident OPCs can give rise to new oligodendrocytes, and in the mouse 30% of the myelin is *de novo* generated by 12 wpi (Assinck et al., 2017b); combined with the increase in P0+ SC myelin during that time, this could explain the increased rim thickness observed. The fact that rim thickness was more pronounced in the SKP-SC large transplant subgroup at 29 wpi may be due to increased axonal growth/regeneration, as that group had a higher number of axons in intact-appearing tissue than either the medium-treated or TofT control groups. In addition, replacement of oligodendrocyte myelin by SC myelin may have contributed to thicker rims (particularly in the SKP-SC group), as SC myelin is known to occupy more space than oligodendrocyte myelin (Kocsis and Waxman, 2007). Whether oligodendrocyte remyelination plays a role in locomotor recovery remains unclear in this study, but a direct role seems unlikely as genetic inhibition of remyelination in mice did not impede spontaneous functional recovery in a comparable moderate contusion injury model (Duncan et al., 2018).

The enhanced endogenous SC response in SKP-SC transplanted animals suggests that the presence, even if transient, of SKP-SCs results in more endogenous myelinating and non-myelinating SCs at the injury epicenter. This agrees with data from experiments transplanting nerve-derived SCs (Biernaskie et al., 2007; Hill et al., 2006), olfactory ensheathing cells (OECs) (Ramer et al., 2004), bone marrow stromal cells (Lu et al., 2007), and fibroblasts (Sparling et al., 2015) after SCI. Our fate-mapping work indicates that most of the SCs observed in the spinal cord of adult mice after contusion injury are derived from CNS OPCs (Assinck et al., 2017b). In agreement, OPCs can become SCs after transplantation (Talbott et al., 2006) or chemical demyelination of the spinal cord in mice, where this phenomenon was primarily observed in areas lacking astrocytes (Zawadzka et al., 2010). Cell-specific deletion of STAT3 in astrocytes decreased remyelination by oligodendrocytes in favor of SCs (Monteiro de Castro et al., 2015), and MBP/WNT signaling within the perivascular niche supports OPC differentiation into SCs after chemical demyelination (Ulanska-Poutanen et al., 2018). Hence, our data suggest that transplanted SKP-SCs may promote the generation of SCs from OPCs in the chronically injured spinal cord.

Few pre-clinical cell transplantation studies have been performed in the chronic stage of spinal cord contusion or compression injuries and efficacy usually required co-treatments (Tetzlaff et al., 2011). No behavioral improvements have been observed after chronic transplantation without co-treatments of, e.g., neural stem cells (Jin et al., 2016; Karimi-Abdolrezaee et al., 2010; Nutt et al., 2013; Parr et al., 2007; Suzuki et al., 2017), OECs (Barakat et al., 2005), or human embryonic stem cell-derived OPCs (Keirstead et al., 2005) when those cells have been applied on their own in "chronic" pre-clinical SCI studies using rodents (i.e., ~2 months or more after injury). Indeed, mouse neural stem/progenitor cells transplanted 7 weeks after clip compression injury in rats required combinatorial administration of chondroitinase ABC, minocycline, plus a cocktail of growth factors to achieve notable functional improvements (Karimi-Abdolrezaee et al., 2010). Similarly, other co-treatments, such as γ-secretase inhibitors, treadmill training, and chondroitinase ABC are improving the

outcomes of transplantation in the early chronic stages (Nori et al., 2018; Okubo et al., 2018; Tashiro et al., 2016). Taken together, the available data suggest that realizing functional improvements after long treatment delays is extremely challenging, particularly for cellular therapies delivered without co-treatments. With that in mind, the functional outcomes seen here with a single-cell therapy, SKP-SCs, applied at 8 wpi were highly encouraging. To our knowledge, only a couple of other chronic (approximately 6–8 wpi) spinal cord contusion studies have demonstrated any functional efficacy for a single-cell therapy in the absence of co-treatments (Barakat et al., 2005; Okubo et al., 2018). One of these studies used SCs generated from peripheral nerves (Barakat et al., 2005). In addition to effects in the open field, our study found benefits in gait performance and reduced signs of bladder pathology for SKP-SC-treated animals.

The present work may represent an important step toward the development of an autologous or allogeneic transplantation protocol to treat chronic SCI with SCs generated from the skin, a highly accessible and available alternative to peripheral nerves. The number of people living with chronic SCI far outweighs the number who might benefit from acute treatments. The functional improvements and mitigation of SCI-related bladder pathology seen in this study after chronic transplantation of SKP-SC are encouraging as any long-term functional gain may have a positive impact on the health of the aging chronic SCI population. Nerve-derived SCs and SKP-SCs at the transcriptome level show only discrete differences between these cell types (Krause et al., 2014), adding credence to the notion that SKP-SCs should perform similarly to their nerve-derived counterparts in clinical trials. However, pre-clinical experiments that address the safety and efficacy of human neonatal/adult SKP-SCs are required to determine whether autologous SKP-SC transplantation merits trials in humans with SCI.

EXPERIMENTAL PROCEDURES

For the full details of all procedures, please see the Supplemental Experimental Procedures. In brief, 47 adult female Sprague-Dawley rats (Charles River, Wilmington, MA) were injured/treated. All procedures were approved by the Hospital for Sick Children Research Institute and the University of British Columbia Animal Care Committee in accordance with the guidelines of the Canadian Council on Animal Care. Behavioral and histological assessments were conducted and analyzed by individuals blinded to treatment. All group comparisons involved parametric or non-parametric analyses. The significance level for all tests was $p < 0.05$; two-tailed.

SCI, Cell Culture, and Transplantation

All rats received a 200-kdyne thoracic contusion SCI at the T9/T10 vertebral level delivered via the Infinite Horizon Impactor (Precision Systems) while deeply anesthetized. As previously described (Biernaskie et al., 2006), primary rat SKPs were prepared from the back skin of neonatal (P0–P3) GFP-expressing Sprague-Dawley rats (SLC, Japan) and differentiated into SKP-SCs. At 8 weeks after SCI, 5 μL of medium alone or containing one million SKP-SCs, was stereotaxically injected into the contusion site. An additional group of rats received SCI only, to characterize the lesion site at TofT (8 wpi). Thirty-eight rats were included in the final analyses and grouped according to treatment as follows: "SKP-SC transplant" (received neonatal SKP-SCs; n = 15), "medium-injected control" (n = 15), and "TofT control" (n = 8).

Functional Assessment

Functional locomotor abilities were assessed using the open field BBB score and subscore, footprint analysis, and the irregular horizontal ladder.

Histological Assessment

SKP-SC- and medium-treated rats were perfused with 4% paraformaldehyde at 29 wpi and the TofT control group was perfused at 8 wpi. Following cryoprotection and freezing, the spinal cords were sectioned longitudinally (each slide containing 10 sagittal sections spaced 200–220 μm apart) and the bladders were cut transversely (each slide containing two cross-sections of the bladder wall), both on a cryostat at 20 μm thickness. Using immunohistochemistry (see Table S1 for list of antibodies), all 10 longitudinal sections were analyzed to calculate lesion volume, transplant volume, P0 volume, P75NTR volume, average intact-appearing tissue, average tissue width, and GFAP intensity. Axon counts and GFP+ graft densities were performed on a subset of spinal cord sections.

For more details, see Supplemental Experimental Procedures.

SUPPLEMENTAL INFORMATION

Supplemental Information can be found online at https://doi.org/10.1016/j.stemcr.2020.05.017.

AUTHOR CONTRIBUTIONS

P.A., J.S.S., J.B., F.D.M., and W.T. designed the research. P.A., J.S.S., S.D., G.J.D., and J.L. performed the experiments. P.A., G.J.D., and D.L.W. analyzed the data. P.A. and W.T. wrote the paper with editorial contributions from J.S.S., G.J.D., B.K.K., J.B., and F.D.M.

ACKNOWLEDGMENTS

The technical assistance of Yuan Jiang, Clarrie Lam, Michael J. Lee, Ailbish Skinner, and Lisa Anderson is gratefully acknowledged. We also thank Dr. Leanne Ramer, Dr. Jason Plemel, and Dr. Brett J. Hilton for their valuable advice. We also acknowledge Dr. J. Trimmer for providing us with nodal antibodies. Graphical abstract created with BioRender.com. We apologize to our colleagues who were not cited due to space limitations. This work was supported by Canadian Institutes of Health Research (CIHR) (130475) and a CIHR Regenerative Medicine and Nanotechnology grant (RMF92085) and the Canadian Stem Cell Network (SCN CT8). P.A. received a CIHR Masters and Doctoral Award; S.D. held a CIHR Training Program in Regenerative Medicine studentship; G.J.D. was supported by an MS Society of Canada Doctoral Scholarship; J.B. held a CIHR

post-doctoral fellowship; B.K.K. holds the Canada Research Chair (CRC) in SCI; F.D.M. is a CRC and a Howard Hughes Medical Institute International Research Scholar; W.T. holds the John and Penny Ryan British Columbia Leadership Chair in Spinal Cord Research.

Received: January 31, 2017
Revised: May 20, 2020
Accepted: May 21, 2020
Published: June 18, 2020

REFERENCES

Anderson, K.D. (2004). Targeting recovery: priorities of the spinal cord-injured population. J. Neurotrauma *21*, 1371–1383.

Anderson, K.D., Guest, J.D., Dietrich, W.D., Bartlett Bunge, M., Curiel, R., Dididze, M., Green, B.A., Khan, A., Pearse, D.D., Saraf-Lavi, E., et al. (2017). Safety of autologous human Schwann cell transplantation in subacute thoracic spinal cord injury. J. Neurotrauma *34*, 2950–2963.

Anderson, M.A., Burda, J.E., Ren, Y., Ao, Y., O'Shea, T.M., Kawaguchi, R., Coppola, G., Khakh, B.S., Deming, T.J., and Sofroniew, M.V. (2016). Astrocyte scar formation aids central nervous system axon regeneration. Nature *532*, 195–200.

Assinck, P., Duncan, G.J., Hilton, B.J., Plemel, J.R., and Tetzlaff, W. (2017a). Cell transplantation therapy for spinal cord injury. Nat. Neurosci. *20*, 637–647.

Assinck, P., Duncan, G.J., Plemel, J.R., Lee, M.J., Stratton, J.A., Manesh, S.B., Liu, J., Ramer, L.M., Kang, S.H., Bergles, D.E., et al. (2017b). Myelinogenic plasticity of oligodendrocyte precursor cells following spinal cord contusion injury. J. Neurosci. *37*, 8635–8654.

Barakat, D.J., Gaglani, S.M., Neravetla, S.R., Sanchez, A.R., Andrade, C.M., Pressman, Y., Puzis, R., Garg, M.S., Bunge, M.B., and Pearse, D.D. (2005). Survival, integration, and axon growth support of glia transplanted into the chronically contused spinal cord. Cell Transplant *14*, 225–240.

Bastidas, J., Athauda, G., De La Cruz, G., Chan, W.M., Golshani, R., Berrocal, Y., Henao, M., Lalwani, A., Mannoji, C., Assi, M., et al. (2017). Human Schwann cells exhibit long-term cell survival, are not tumorigenic and promote repair when transplanted into the contused spinal cord. Glia *65*, 1278–1301.

Biernaskie, J., Sparling, J.S., Liu, J., Shannon, C.P., Plemel, J.R., Xie, Y., Miller, F.D., and Tetzlaff, W. (2007). Skin-derived precursors generate myelinating Schwann cells that promote remyelination and functional recovery after contusion spinal cord injury. J. Neurosci. *27*, 9545–9559.

Biernaskie, J.A., McKenzie, I.A., Toma, J.G., and Miller, F.D. (2006). Isolation of skin-derived precursors (SKPs) and differentiation and enrichment of their Schwann cell progeny. Nat. Protoc. *1*, 2803–2812.

Boerboom, A., Dion, V., Chariot, A., and Franzen, R. (2017). Molecular mechanisms involved in Schwann cell plasticity. Front. Mol. Neurosci. *10*, 38.

Bunge, M.B. (2016). Efficacy of Schwann cell transplantation for spinal cord repair is improved with combinatorial strategies. J. Physiol. *594*, 3533–3538.

Bunge, M.B., Monje, P.V., Khan, A., and Wood, P.M. (2017). From transplanting Schwann cells in experimental rat spinal cord injury to their transplantation into human injured spinal cord in clinical trials. Prog. Brain Res. *231*, 107–133.

Bunge, R.P. (1994). The role of the Schwann cell in trophic support and regeneration. J. Neurol. *242*, S19–S21.

de Groat, W.C., Kawatani, M., Hisamitsu, T., Cheng, C.L., Ma, C.P., Thor, K., Steers, W., and Roppolo, J.R. (1990). Mechanisms underlying the recovery of urinary bladder function following spinal cord injury. J. Auton. Nerv Syst. *30 Suppl*, S71–S77.

Deng, L.X., Deng, P., Ruan, Y., Xu, Z.C., Liu, N.K., Wen, X., Smith, G.M., and Xu, X.M. (2013). A novel growth-promoting pathway formed by GDNF-overexpressing Schwann cells promotes propriospinal axonal regeneration, synapse formation, and partial recovery of function after spinal cord injury. J. Neurosci. *33*, 5655–5667.

Dias, D.O., Kim, H., Holl, D., Werne Solnestam, B., Lundeberg, J., Carlen, M., Goritz, C., and Frisen, J. (2018). Reducing pericyte-derived scarring promotes recovery after spinal cord injury. Cell *173*, 153–165 e122.

Duncan, G.J., Manesh, S.B., Hilton, B.J., Assinck, P., Liu, J., Moulson, A., Plemel, J.R., and Tetzlaff, W. (2018). Locomotor recovery following contusive spinal cord injury does not require oligodendrocyte remyelination. Nat. Commun. *9*, 3066.

Filous, A.R., and Silver, J. (2016). Targeting astrocytes in CNS injury and disease: a translational research approach. Prog. Neurobiol. *144*, 173–187.

Hill, C.E., Moon, L.D., Wood, P.M., and Bunge, M.B. (2006). Labeled Schwann cell transplantation: cell loss, host Schwann cell replacement, and strategies to enhance survival. Glia *53*, 338–343.

Hoke, A., Redett, R., Hameed, H., Jari, R., Zhou, C., Li, Z.B., Griffin, J.W., and Brushart, T.M. (2006). Schwann cells express motor and sensory phenotypes that regulate axon regeneration. J. Neurosci. *26*, 9646–9655.

Hood, B., Levene, H.B., and Levi, A.D. (2009). Transplantation of autologous Schwann cells for the repair of segmental peripheral nerve defects. Neurosurg. Focus *26*, E4.

Illes, J., Reimer, J.C., and Kwon, B.K. (2011). Stem cell clinical trials for spinal cord injury: readiness, reluctance, redefinition. Stem Cell Rev. Rep. *7*, 997–1005.

Jin, Y., Bouyer, J., Shumsky, J.S., Haas, C., and Fischer, I. (2016). Transplantation of neural progenitor cells in chronic spinal cord injury. Neuroscience *320*, 69–82.

Karimi-Abdolrezaee, S., Eftekharpour, E., Wang, J., Schut, D., and Fehlings, M.G. (2010). Synergistic effects of transplanted adult neural stem/progenitor cells, chondroitinase, and growth factors promote functional repair and plasticity of the chronically injured spinal cord. J. Neurosci. *30*, 1657–1676.

Keirstead, H.S., Nistor, G., Bernal, G., Totoiu, M., Cloutier, F., Sharp, K., and Steward, O. (2005). Human embryonic stem cell-derived oligodendrocyte progenitor cell transplants remyelinate and restore locomotion after spinal cord injury. J. Neurosci. *25*, 4694–4705.

Kocsis, J.D., and Waxman, S.G. (2007). Schwann cells and their precursors for repair of central nervous system myelin. Brain *130*, 1978–1980.

Krause, M.P., Dworski, S., Feinberg, K., Jones, K., Johnston, A.P., Paul, S., Paris, M., Peles, E., Bagli, D., Forrest, C.R., et al. (2014). Direct genesis of functional rodent and human Schwann cells from skin mesenchymal precursors. Stem Cell Reports *3*, 85–100.

Lu, P., Jones, L.L., and Tuszynski, M.H. (2007). Axon regeneration through scars and into sites of chronic spinal cord injury. Exp. Neurol. *203*, 8–21.

Monteiro de Castro, G., Deja, N.A., Ma, D., Zhao, C., and Franklin, R.J. (2015). Astrocyte activation via Stat3 signaling determines the balance of oligodendrocyte versus Schwann cell remyelination. Am. J. Pathol. *185*, 2431–2440.

Nori, S., Khazaei, M., Ahuja, C.S., Yokota, K., Ahlfors, J.E., Liu, Y., Wang, J., Shibata, S., Chio, J., Hettiaratchi, M.H., et al. (2018). Human oligodendrogenic neural progenitor cells delivered with chondroitinase ABC facilitate functional repair of chronic spinal cord injury. Stem Cell Reports *11*, 1433–1448.

Nutt, S.E., Chang, E.A., Suhr, S.T., Schlosser, L.O., Mondello, S.E., Moritz, C.T., Cibelli, J.B., and Horner, P.J. (2013). Caudalized human iPSC-derived neural progenitor cells produce neurons and glia but fail to restore function in an early chronic spinal cord injury model. Exp. Neurol. *248*, 491–503.

Okubo, T., Nagoshi, N., Kohyama, J., Tsuji, O., Shinozaki, M., Shibata, S., Kase, Y., Matsumoto, M., Nakamura, M., and Okano, H. (2018). Treatment with a gamma-secretase inhibitor promotes functional recovery in human iPSC-derived transplants for chronic spinal cord injury. Stem Cell Reports *11*, 1416–1432.

Parr, A.M., Kulbatski, I., and Tator, C.H. (2007). Transplantation of adult rat spinal cord stem/progenitor cells for spinal cord injury. J. Neurotrauma *24*, 835–845.

Pearse, D.D., Bastidas, J., Izabel, S.S., and Ghosh, M. (2018). Schwann cell transplantation subdues the pro-inflammatory innate immune cell response after spinal cord injury. Int. J. Mol. Sci. *19*, 2550.

Ramer, L.M., Au, E., Richter, M.W., Liu, J., Tetzlaff, W., and Roskams, A.J. (2004). Peripheral olfactory ensheathing cells reduce scar and cavity formation and promote regeneration after spinal cord injury. J. Comp. Neurol. *473*, 1–15.

Sparling, J.S., Bretzner, F., Biernaskie, J., Assinck, P., Jiang, Y., Arisato, H., Plunet, W.T., Borisoff, J., Liu, J., Miller, F.D., et al. (2015). Schwann cells generated from neonatal skin-derived precursors or neonatal peripheral nerve improve functional recovery after acute transplantation into the partially injured cervical spinal cord of the rat. J. Neurosci. *35*, 6714–6730.

Suzuki, H., Ahuja, C.S., Salewski, R.P., Li, L., Satkunendrarajah, K., Nagoshi, N., Shibata, S., and Fehlings, M.G. (2017). Neural stem cell mediated recovery is enhanced by Chondroitinase ABC pretreatment in chronic cervical spinal cord injury. PLoS One *12*, e0182339.

Talbott, J.F., Cao, Q., Enzmann, G.U., Benton, R.L., Achim, V., Cheng, X.X., Mills, M.D., Rao, M.S., and Whittemore, S.R. (2006). Schwann cell-like differentiation by adult oligodendrocyte precursor cells following engraftment into the demyelinated spinal cord is BMP-dependent. Glia *54*, 147–159.

Tashiro, S., Nishimura, S., Iwai, H., Sugai, K., Zhang, L., Shinozaki, M., Iwanami, A., Toyama, Y., Liu, M., Okano, H., et al. (2016). Functional recovery from neural stem/progenitor cell transplantation combined with treadmill training in mice with chronic spinal cord injury. Sci. Rep. *6*, 30898.

Tetzlaff, W., Okon, E.B., Karimi-Abdolrezaee, S., Hill, C.E., Sparling, J.S., Plemel, J.R., Plunet, W.T., Tsai, E.C., Baptiste, D., Smithson, L.J., et al. (2011). A systematic review of cellular transplantation therapies for spinal cord injury. J. Neurotrauma *28*, 1611–1682.

Toma, J.G., Akhavan, M., Fernandes, K.J., Barnabe-Heider, F., Sadikot, A., Kaplan, D.R., and Miller, F.D. (2001). Isolation of multipotent adult stem cells from the dermis of mammalian skin. Nat. Cell Biol. *3*, 778–784.

Ulanska-Poutanen, J., Mieczkowski, J., Zhao, C., Konarzewska, K., Kaza, B., Pohl, H.B., Bugajski, L., Kaminska, B., Franklin, R.J., and Zawadzka, M. (2018). Injury-induced perivascular niche supports alternative differentiation of adult rodent CNS progenitor cells. eLife *7*, e30325.

Wiliams, R.R., and Bunge, M.B. (2012). Schwann cell transplantation: a repair strategy for spinal cord injury? Prog. Brain Res. *201*, 295–312.

Williams, R.R., Henao, M., Pearse, D.D., and Bunge, M.B. (2015). Permissive Schwann cell graft/spinal cord interfaces for axon regeneration. Cell Transplant *24*, 115–131.

Zawadzka, M., Rivers, L.E., Fancy, S.P., Zhao, C., Tripathi, R., Jamen, F., Young, K., Goncharevich, A., Pohl, H., Rizzi, M., et al. (2010). CNS-resident glial progenitor/stem cells produce Schwann cells as well as oligodendrocytes during repair of CNS demyelination. Cell Stem Cell *6*, 578–590.

Stem Cell Reports, Volume *15*

Supplemental Information

Transplantation of Skin Precursor-Derived Schwann Cells Yields Better Locomotor Outcomes and Reduces Bladder Pathology in Rats with Chronic Spinal Cord Injury

Peggy Assinck, Joseph S. Sparling, Shaalee Dworski, Greg J. Duncan, Di L. Wu, Jie Liu, Brian K. Kwon, Jeff Biernaskie, Freda D. Miller, and Wolfram Tetzlaff

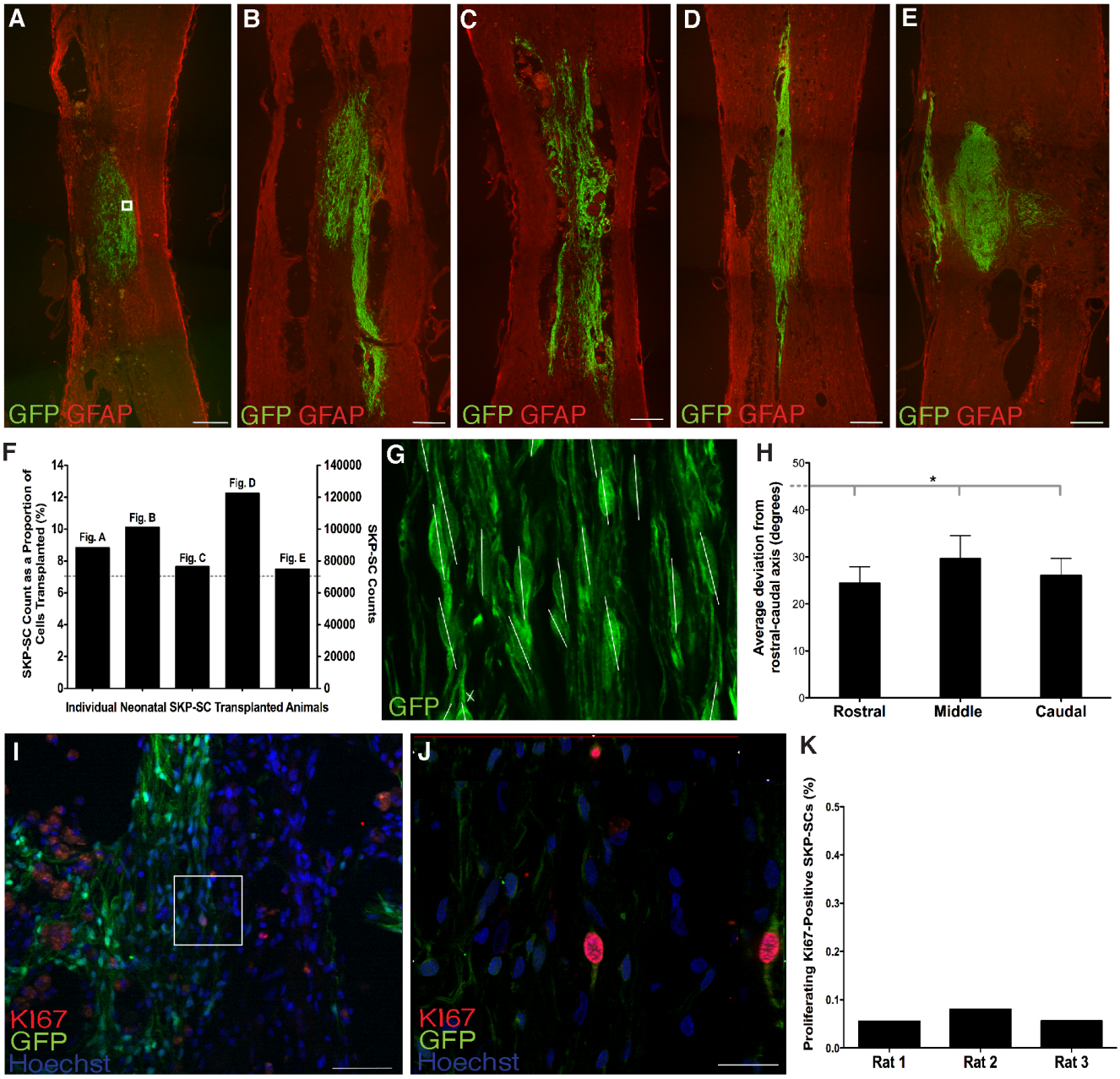
A
B
C
D
E
GFP GFAP
F
SKP-SC Count as a Proportion of Cells Transplanted (%)
SKP-SC Counts
Fig. A
Fig. B
Fig. C
Fig. D
Fig. E
Individual Neonatal SKP-SC Transplanted Animals
G
GFP
H
Average deviation from rostral-caudal axis (degrees)
Rostral
Middle
Caudal
I
KI67
GFP
Hoechst
J
KI67
GFP
Hoechst
K
Proliferating KI67-Positive SKP-SCs (%)
Rat 1
Rat 2
Rat 3

Figure S1. SKP-SCs show a predominantly rostral-caudal orientation and a low incidence of proliferation at 21 weeks post transplantation. Related to Figure 1. (A-E) Photomicrographs of GFAP-immunostained contused spinal cords from the five animals that make up the large transplant SKP-SC 'sub-group' (see Supplemental Experimental Procedures) at 29 wpi used for quantification in Figure S1-3 and axon count analysis (Figure 3). Note that the SKP-SCs integrate into the lesion sites and bridge the cavity. (**F**) SKP-SC counts at 29 wpi for the rats in the large transplant sub-group. Each bar corresponds to the appropriate image shown above (A-E) and is a subset (>70000 cells) of those shown in Figure 1F. **(G)** Photomicrograph of box shown in A demonstrating the associated vectors assigned to each transplanted GFP+ SKP-SC in the orientation analysis. Note that 'x' marks cells that were given a 90-degree value signifying they were coming out of the plane**. (H)** Quantification demonstrating that the majority of transplanted SKP-SCs displayed a strong rostral-caudal orientation at the rostral, middle and caudal regions of the graph as demonstrated by an average deviation from rostral–caudal axis (0 degrees) of 26 degrees. The rostral, middle and caudle deviations were significantly less than 45 degrees (representative of an average random orientation; **p*<0.027; t-test; n=5). **(I)** Photomicrograph demonstrating the low number of transplanted GFP+ SKP-SCs that co-localized with the proliferative marker KI67 at 29 wpi**. (J)** Confocal image taken at the location of the box in I demonstrating clear co-localization of Hoechst and KI67 in the nucleus of a GFP+ SKP-SC. **(K)** To assess proliferation of the transplanted SKP-SC at 29 wpi, we quantified the percentage of GFP+ cells that expressed the marker KI67. Only 0.05% of the cells were KI67+, suggesting minimal proliferation of SKP-SCs at 21 weeks after transplant. This KI67 proliferative index is lower than in benign Schwannomas (average of 1.2% KI67+ cells) and malignant peripheral nerve sheath tumors (average of 23% KI67-positive cells; Ghilusi et al., 2009). Accordingly, there was no indication of SKP-SC derived malignancy in our grafts. Scale bars: 200 μm in A-E, 50 μm in G & I, and 20 μm in J. Data are presented as individual data for F (n=5) and K (n=3) and group means +/- SEM for H (n=5).

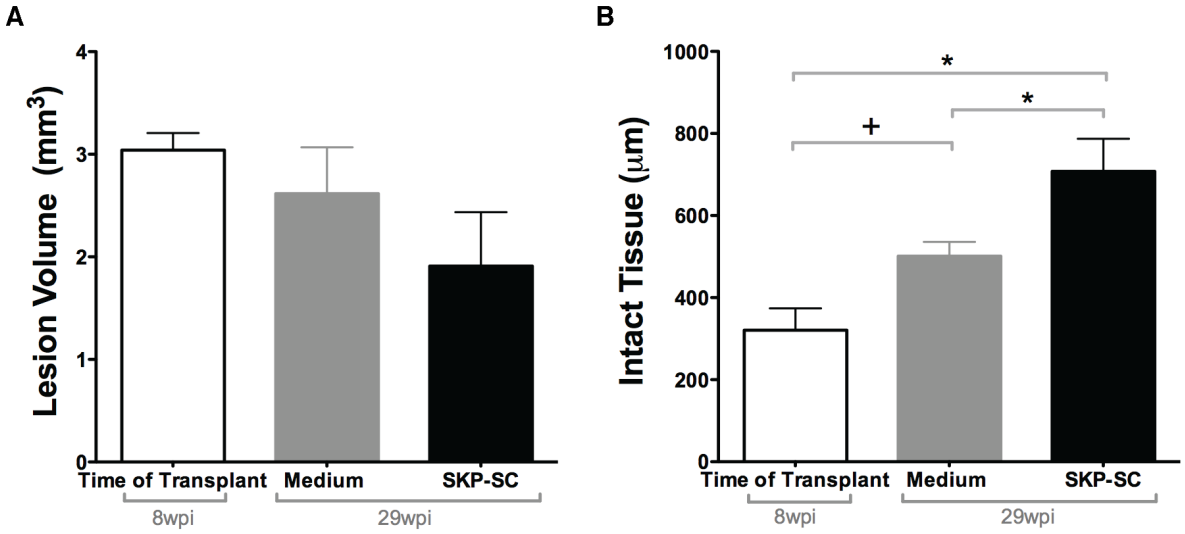

Figure S2. High SKP-SC survival results in more intact tissue than in control animals. Related to Figure 1. **(A)** The mean lesion volume for animals with high transplant cell survival and their appropriate controls is similar among the three groups. **(B)** Mean intact GFAP+ tissue (spared rim and tissue bridges included) showed significant differences among the sub-groups. Note the significantly larger intact tissue in the SKP-SC sub-group with high transplant survival compared to the medium (*p=0.029; ANOVA with LSD) and time of transplant (TofT) control (*p=0.001; ANOVA with LSD) sub-groups. Also, the amount of intact tissue in the medium injected sub-group compared to the TofT control sub-group approached statistical significance (+p=0.051; ANOVA with LSD). Sub-group analysis: SKP-SC n=5; Medium n=5; TofT n=5. All data presented as mean +/- SEM.

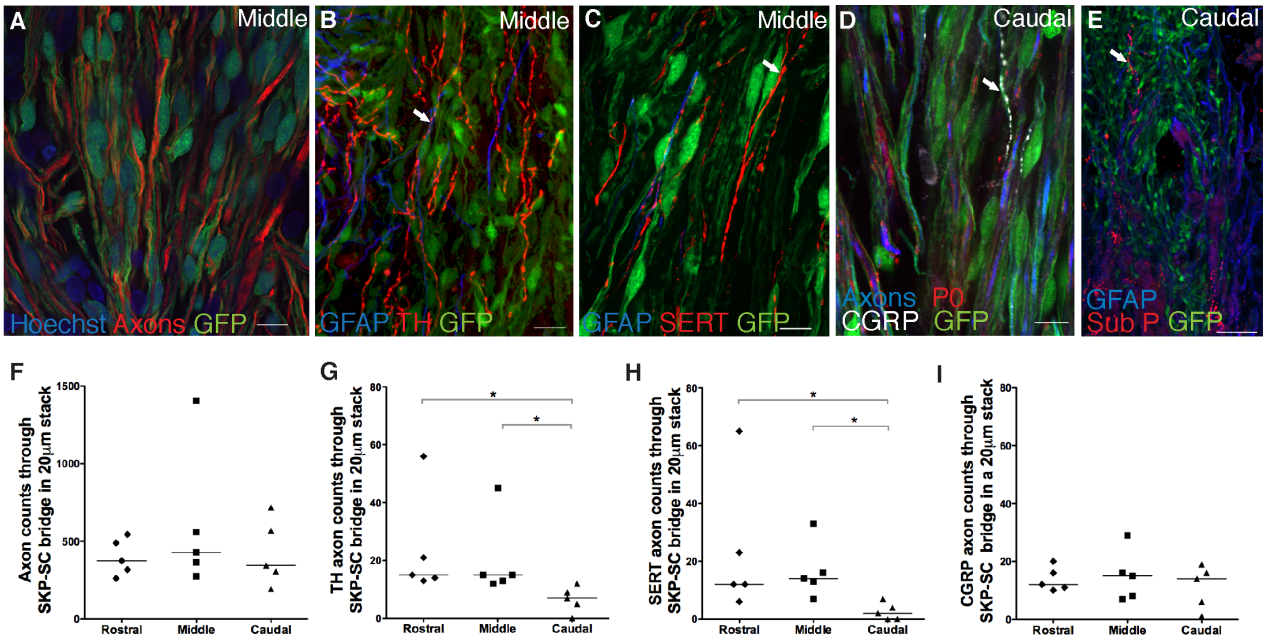

Figure S3. Significantly more TH- and SERT+ axons at the rostral and middle levels of the SKP-SC bridge compared to the caudal levels. Related to Figure 3. Representative photomicrographs depicting NF200/βIII-TUBULIN+ **(A),** TH+ **(B),** SERT+ **(C)**, CGRP+ **(D)**, and Substance P+ **(E)** axons growing through GFP+ SKP-SC bridges. **(F-I)** Quantifications of NF200/βIII-Tubulin+ (F), TH+ (G), SERT+ (H) and CGRP+ (I) axon counts at rostral, middle, and caudal levels (yellow lines in Figure 3E) of the spinal cord in five animals from the SKP-SC sub-group. There were significantly more TH+ and SERT+ axons at the rostral and middle levels of the SKP-SC bridges than at the caudal level (all *p<0.05; Friedman test with follow up Wilcoxon) supporting the interpretation of rostral to caudal regeneration of these brainstem-derived axons. Sub-group analysis: SKP-SC n=5; Medium n=5; TofT n=5. Scale bars: 50 μm for E; 20 μm for B; 10 μm for A,C,D. Individual data points for each animal are presented with group medians indicated by solid black lines in F-I.

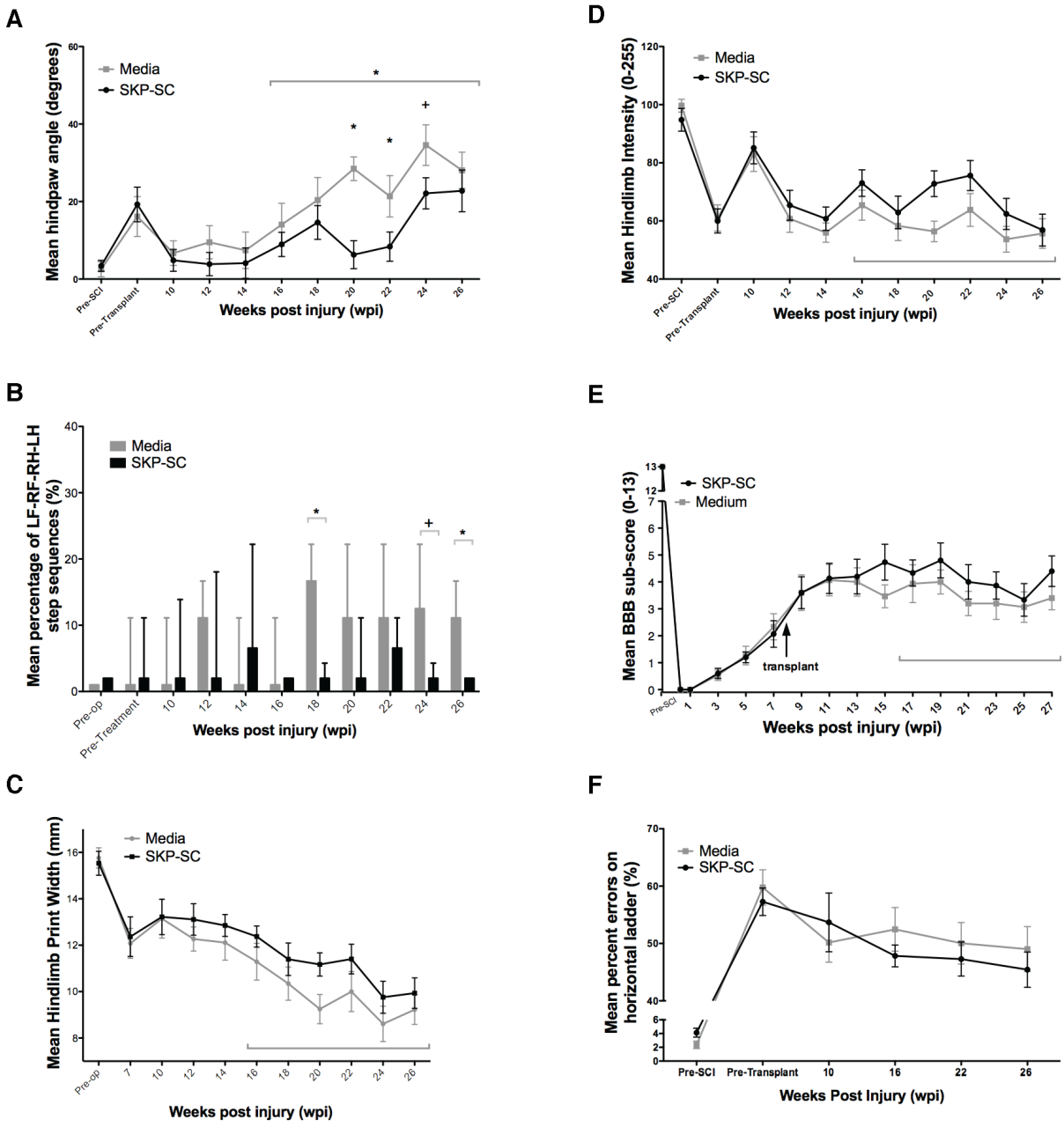

Figure S4. SKP-SCs elicited functional improvements on paw angle and step sequence parameters on the CatWalk. Related to Figure 6. (**A**) SKP-SC transplanted animals showed a significantly lower paw angle (less outward rotation) over the last 10 weeks of behavior, as indicated by a significant interaction (**p*=0.041; repeated measures ANOVA). Follow-up analysis indicated that the SKP-SC group had significantly lower paw angles at 20 and 22 wpi (**p*<0.047; t-test) and a trend at 24 wpi (+*p*=0.072; t-test) but this difference was not maintained at 26 wpi. **(B)** The SKP-SC transplanted group showed a significantly smaller percentage of the abnormal stepping pattern LF-RF-RH-LH as compared to the medium control group at week 18 and 26 (**p*<0.003; MWU) and approached significance at week 24 (+*p*=0.076). There were no significant interactions found on the repeated measures ANOVA in mean hindlimb print width **(C)** or mean hindlimb intensity **(D)** CatWalk parameters or the mean BBB subscore **(E)** or the irregular horizontal ladder **(F).** SKP-SC n=15; Medium n=15. Data is presented as means +/- SEM**.**

Antibody	Source	Concentration
mouse anti-S100β	Sigma-Aldrich, St. Louis, MO **AMAB91038**	1:500
rabbit anti-GFAP	Dako, Glostrup, Denmark **Z0334**	1:1000
goat anti-GFAP	Santa Cruz Biotechnology, Santa Cruz, CA **sc-6170**	1:50
mouse anti-GFAP	Sigma-Aldrich, St. Louis, MO **G3893**	1:500
chicken anti-P0	Aves, Tigard OR **PZ0**	1:100
chicken anti-GFP	Millipore, Billerica, MA **AB16901**	1:1000
rabbit anti-GFP	Millipore, Billerica, MA **AB3080**	1:100
goat anti-GFP	Rockland Immunochemicals, Gilbertsville, PA **600-101-215**	1:200
mouse anti-GFP	Millipore, Billerica, MA **Mab3580**	1:500
mouse anti-neurofilament 200 (NF-200)	Sigma-Aldrich, St. Louis, MO **N0142**	1:500
rabbit anti-NF-200	AbD Serotec, Releigh, NC **AHP245**	1:1000
mouse anti-ßIII-Tubulin	Sigma-Aldrich, St. Louis, MO **T8660**	1:500
rabbit anti-βIII- Tubulin	Covance, Princeton, NJ **PRB-435P**	1:500
rabbit anti-serotonin transporter (SERT)	Immunostar, Hudson, WI **24330**	1:500
sheep anti-tyrosine hydroxylase (TH)	Millipore, Billerica, MA **AB1542**	1:200
rabbit anti-calcitonin gene-related peptide (CGRP)	Sigma-Aldrich, St. Louis, MO **C8198**	1:500
rabbit anti-Substance P	Millipore, Billerica, MA **AB1566**	1:500
mouse anti-P75NTR	Millipore, Billerica, MA **MAB357**	1:500
rabbit anti-laminin	Sigma-Aldrich, St. Louis, MO **L9393**	1:200
mouse anti-neurocan	Developmental Studies Hybridoma Bank, Iowa City, IO; **ID1**	1:100
mouse anti-chondrontin sulfate proteoglycan (CS56)	Sigma-Aldrich, St. Louis, MO **C8035**	1:200
mouse anti-KV1.2 potassium channels	Generous gift from Dr. J. Trimmer, University of California, Davis, CA	1:200
mouse anti-contactin-associated protein (CASPR)	Generous gift from Dr. J. Trimmer, University of California, Davis, CA	1:300
mouse anti-KI67	BD Biosciences, Mississauga, ON **550609**	1:20
Rabbit anti-IBA1	FUJIFILM Wako Pure Chemical Corporation, Osaka Japan; **019-19741**	1:5000

Table S1. List of primary antibodies used. Related to main text Experimental Procedures. Antibody host, source and concentration specific to immunohistochemistry are shown.

Compared Parameters	Correlation Coefficient	P Value
Intact Tissue vs. P0+ve Volume	r=0.502	* p<0.001
Intact Tissue vs. P0+ve Volume Inside Lesion	r=0.429	* p=0.009
Intact Tissue vs. P0+ve Volume Outside Lesion	r=0.557	* p<0.001
Intact Tissue vs. Total Axons	r=0.782	* p=0.001 ϕ
Intact Tissue vs. P75NRT+ve Volume	r=0.388	* p=0.042
Intact Tissue vs. SERT+ Axons	r=0.804	* p=0.000 ϕ
Intact Tissue vs. TH+ Axons	r=0.720	* p=0.004 ϕ
Intact Tissue vs. Lesion Volume	r=-0.469	* p=0.004
P0+ve Volume Outside Lesion vs. 27wpi BBB	ρ =0.648	* p=0.009
P0+ve Volume vs. Total Axons	r=0.492	+ p=0.063 ϕ
P0+ve Volume vs. SERT+ve Axons	r=0.512	+ p=0.051 ϕ
P0+ve Volume vs. TH+ve Axons	r=0.463	+ p=0.080 ϕ
P75NTR+ve Volume vs. SERT+ve Axons	r=0.677	* p=0.031 ϕ
P75NTR+ve Volume vs. TH+ve Axons	r=0.739	* p=0.015 ϕ
BBB 27wpi vs. Ladder % Error 26wpi	ρ =-0.358	+ p=0.052
GFAP Max Value vs. Cavity Volume	r=0.448	* p=0.006
Bladder Wet Weight vs. 27wpi BBB	ρ =-0.501	* p=0.004
Bladder Wet Weight vs 27wpi BBB subscore	ρ =-0.582	* p<0.001

*** Significance p<0.05 + p=0.05-0.1 ϕ Correlations run with sub-groups (n=5).**

Table S2. List of relevant compared significant correlations. Related to Figure 1-6.

Supplemental Experimental Procedures: Related to Experimental Procedures.

Animals

Forty-seven adult female *Sprague Dawley* rats (295±10g; Charles River Laboratories, Wilmington WA) were used in this study. All procedures were approved by the Hospital for Sick Children Research Institute and the University of British Columbia Animal Care Committee in accordance with the guidelines of the Canadian Council on Animal Care. Animals were housed in a room with a reverse light/dark cycle with free access to food and water throughout the study.

Spinal Cord Contusion Injury

Rats received buprenorphine (0.03mg/kg, s.c.) pre-operatively and were anaesthetized with isofluorane (4% induction, ~1.5% maintenance); body temperature was maintained at 36.5±0.5°C. Lidocaine (0.5ml) with 2% epinephrine was injected at the surgical site for additional analgesia and vasoconstriction. The spinal cord was exposed via a thoracic midline incision between T6 and L1 and a laminectomy at vertebra T9 under strictly aseptic conditions. The T8 and T10 dorsal vertebral processes were stabilized with Allen clamps and a 200 Kdyne force-controlled contusion was delivered with an Infinite Horizon (IH) impactor (Precision Systems, Lexington, KY; Scheff et al., 2003). Following injury, muscle and skin were sutured in layers. Lactated Ringers solution (10ml, s.c.) was administered every 12 hours for two days to prevent dehydration. Bladders were manually expressed three times daily until spontaneous micturition returned. Antibiotics (Baytril; 10mg/kg, s.c.) were administered as needed to treat minor bladder infections.

Following injury, three rats were euthanized due to injury-related complications and three rats were excluded from the study prior to treatment, based on spontaneous recovery and injury parameters. We excluded animals that were outliers in terms of injury severity; specifically, we removed animals with the Basso, Beattie, and Bresnahan (BBB) score or subscore at 7 weeks post-injury (wpi) that was >2 standard deviations discrepant from the mean. We also removed animals in which area under the force curve (measured by the Infinite Horizon Impactor) was >2 standard deviations from the mean. Injured rats (n=31) were divided into two groups that were matched based on peak force of injury, area under the force curve, maximum impactor displacement, pre-injury weight, weight prior to transplant, and BBB scores and BBB subscores at 2 days' post-injury and for each subsequent week prior to transplantation. One group was randomly chosen to receive cell treatment (n=15) and the other medium only (n=16) and investigators were blinded to which animals were given either a cell treatment or medium injection. An additional group of rats received the same 200 Kdyne contusion without treatment to form a time of transplant (TofT) control group (n=10); two animals were excluded from this group because the area under the force curve or BBB scores were >2 standard deviations from the pre-treatment group mean used previously.

SKP Isolation and Differentiation into SKP-SCs

As previously described (Biernaskie et al., 2009; Fernandes et al., 2004; Toma et al., 2001; Toma et al., 2005), neonatal primary rat skin-derived precursors (SKPs) were prepared from the back skin of either neonatal (P0-P3) transgenic *Sprague-Dawley* rats that expressed GFP in all cells (SLC, Japan). Secondary spheres were generated by digesting SKPs with collagenase (1mg/ml) then mechanically dissociating to liberate single cells, which were sub-cultured at a density of 35,000-50,000 cells/ml in flasks. Cells were grown at 37ºC and 5% CO_2, fed with SKP proliferation medium (Dulbecco's Modified Eagle's Medium, DMEM:F-12; 3:1; Invitrogen, Carlsbad, CA) containing 1% penicillin/streptomycin (Cambrex, East Rutherford, NJ), 2% B27 supplement (Invitrogen), 20 ng/ml epidermal growth factor (EGF; BD Biosciences, Bedford, MA), and 40 ng/ml fibroblast growth factor 2 (FGF2; BD Biosciences) every 5 days, and passaged every 10 days.

Schwann cells (SC) were differentiated from passage three neonatal SKPs as previously described (Biernaskie et al., 2007; Biernaskie et al., 2006; McKenzie et al., 2006). After two or three passages, purified SKP-SCs were frozen in 90% fetal bovine serum / 10% dimethyl sulfoxide at -80ºC for long-term storage. Approximately 2 weeks prior to transplantation, the SKP-SCs were thawed, plated, and expanded under SC proliferation medium [DMEM/F12 (3:1), 1% penicillin/streptomycin, 2% N2 supplement (Invitrogen), 25 ng/ml neuregulin-1β (R&D Systems, Minneapolis, MN), and 5 μM forskolin (Sigma-Aldrich, St. Louis, MO)]. To investigate the expression of typical SCs markers in the SKP-SC cultures, the cells were fixed for 15 min in 4% paraformaldehyde and stained for GFP, S100B and

Hoechst 33258 (1:1000, Sigma-Aldrich) was used to visualize nuclei. Images were captured via a Zeiss Axiovert 200 spinning disk confocal microscope (Yokogawa, Sugar Land, TX) and C9100-13 EM-CCD camera (Hamamatsu, San Jose, CA), with Volocity acquisition software. SC purity was expressed as the percentage of cells positive for S100β, and the total cell number was determined by Hoechst staining. Four different culture samples were used to determine the purity of neonatal and at least three fields of view were selected randomly (i.e., while visualizing Hoechst) for each sample.

Cell Transplantation

For transplantation at 8 wpi, SKP-SCs were removed from laminin/poly-d-lysine (PDL)-coated plates/flasks by gentle agitation and spraying after 3-5 minute incubation in 0.25% Trypsin/ethylenediaminetetraacetic acid (EDTA). Trypsin was inactivated with 10% fetal bovine serum and cells were triturated gently to produce a single cell suspension, which was then centrifuged (1000 rpm, 5 min.) and re-suspended at 200,000 cells/μl in fresh DMEM:F12 (3:1). Prior to transplantation, rats were anaesthetized and prepared for surgery as outlined above. The laminectomy at T9 was re-exposed and scar tissue was removed to allow access to the site of SCI. One million neonatal SKP-SCs in 5 μl of medium was stereotaxically injected directly into the epicenter of the contusion site using a 10 μl Hamilton syringe fitted with a glass micropipette (~80 μm tip size). Cyclosporine A was delivered to all animals in homecage drinking water (150 mg/l of water; Neoral; Novartis) beginning 4 days before transplantation and continuing for the duration of the study. Oral administration was replaced with injectable cyclosporine A for 4 days post-transplantation (Sandimmune, Novartis; 15mg/kg, s.c.). One medium injected animal was euthanized in the 5 days following the transplantation surgery due to bladder complications (final n=15).

Behavioural Assessments

All behavioral raters were blind to the treatment groups. Functional locomotor abilities were assessed bi-weekly using the open-field BBB score and subscore; (Basso, 2004; Basso et al., 1995), footprint analysis (CatWalk, Noldus, Netherlands; (Hamers et al., 2001), and the irregular horizontal ladder (Metz and Whishaw, 2002). All animals were acclimatized to the testing environment/equipment and trained prior to collection of baseline behavioural data, which were collected during the week prior to SCI. The animals were given two days to recover from SCI before open field-testing resumed, and seven weeks to regain consistent weight supported stepping prior to resuming Catwalk and ladder testing. Animals were further acclimatized to CatWalk and ladder apparatuses prior to the collection of 7 wpi pre-treatment baseline data. The animals were given one week to recover from transplantation surgery before open field-testing resumed and two weeks before CatWalk and ladder testing resumed. From that point onward, all locomotor tests were conducted bi-weekly at the same time of day by the same investigator until 27 wpi.

Open Field Locomotion (BBB).
Open field locomotion was scored on the BBB scale (Basso et al., 1995), and BBB subscale (Basso, 2004). Two raters assigned a score at the time of testing and all animals scored a 21 on the BBB and a 13 on the BBB subscore during pre-injury baseline assessments.

CatWalk.
The CatWalk system (Noldus, Netherlands), enables objective assessment of locomotion parameters based on quantitative footprint data (Hamers et al., 2001; Vrinten and Hamers, 2003). Unusable runs were identified based on the following criteria: 1) running at an inconsistent speed, 2) stopping in the middle of the run, 3) running exceptionally fast or slow. At least five runs were recorded for each rat during each testing session, and three runs were selected by a rater based on consistency of the run and the inclusion of three complete uninterrupted step cycles. The following parameters were examined: forelimb and hindlimb stride length, hindlimb paw angle, hindlimb paw width, hindlimb paw print intensity, and overall step sequence patterns. CatWalk footprint analysis assessing forelimb and hindlimb stride length was normalized to pre-transplant values.

Irregular Horizontal Ladder.
Hindlimb stepping was also assessed using the irregular horizontal ladder (Metz and Whishaw, 2002). Animals were trained to cross the ladder toward their home cage and each crossing was recorded using a high definition digital camera (Sony, Toronto, Canada) for subsequent scoring. The ladder always included the same number of overall rungs and spaces (ranging from one-five missing rungs per space), but the rung positions were changed for each

testing session to avoid any training effects. A frame-by-frame analysis of video recordings of hindlimb stepping yielded error scores (averaged over five trials per session per animal) for the number of overall steps and errors for each hind paw (Metz and Whishaw, 2002).

Tissue Processing

Prior to euthanasia and transcardial perfusion, the bladder of each rat was emptied by manual expression. The TofT control group was euthanized at 8 wpi, whereas the SKP-SC- and medium-treated rats were euthanized at 29 wpi. All rats were overdosed with ketamine (210 mg/kg, i.p.) and xylazine (30 mg/kg, i.p.) and transcardially perfused with 0.12M PBS followed by 4% paraformaldehyde in PBS (0.1M). The thoracic spinal cord encompassing the injury site and the bladder were removed, post-fixed overnight in 4% paraformaldehyde, cryoprotected overnight in 12, 18, and then 24% sucrose in 0.12M PBS, frozen on dry ice and stored frozen at -80°C. The thoracic spinal cord was sectioned longitudinally in the sagittal plane with 10 sets of slides with each slide containing 10 spinal cord sections 200 μm from dorsal to ventral. The bladder was sectioned transversely twice 200 μm apart through the midline. Generally, the central canal was used to determine the center section (mid-sagittal plane) to align equal tissue on both sides for analysis. Both the spinal cord and bladder sections were cut at a thickness of 20 μm using a Microm cryostat (Heidelberg, Germany) onto Superfrost Plus slides (Fisher, Houston, TX) and stored at -80°C.

Immunohistochemistry

Tissue sections were permeabilized with 0.1% Triton-X-100 and treated with 10% donkey serum for 30 min to prevent non-specific binding. For immunolabeling of myelin proteins, brief delipidation was also performed, using graded ethanol solutions prior to the blocking step. For a list of the primary antibodies used, see Table S1. The secondary antibodies were generated in donkey or goat, conjugated with Dylight fluorochromes 405, 488, 594 or 649, and used at a concentration of 1:200 (Jackson ImmunoResearch Laboratories, West Grove, PA). Nuclei were stained with Hoechst 33342 (1:5000).

Histological Quantifications

A Zeiss (Oberkochen, Germany) Axioplan 2 microscope fitted with image acquisition software (Northern Eclipse; Empix, Mississauga, Canada) was used for low magnification images. For higher magnification images, including those used for cell counts, axon counts, and confirmation of co-localization, images were captured on a Zeiss AxioObserver Z1 (Zeiss, Germany) confocal microscope fitted with a CSU-X1 Yokogawa spinning disc and solid-state lasers with 405, 488, 565 and 639 wavelengths. All image analysis was completed by individuals blind to treatment. Associated with this, the green channel (with GFP+ cells) was not provided to the individuals assessing histological outcomes except when necessary; e.g., for GFP+ cell counts and GFP+ volume analyses. Images were merged using Photoshop CS2 or CS4 (Adobe, San Jose, CA). All measurements (e.g., distances, areas, and intensities) except cell/axon counts and vector analysis were performed with Sigma Scan Pro 5 (Systat, Chicago, IL).

Among SKP-SC-treated rats, we defined a sub-group of five animals with very successful survival of transplanted cells (defined by more than 70,000 cells present; see Figure 1F; Figure S1) and compared them to a matched (by injury force/displacement and pre-transplant behavioral parameters) medium-treated sub-group (n=5) and a matched TofT sub-group (n=5). This sub-group analysis was conducted to see whether long-term survival of grafted cells is required for specific observed benefits (e.g., lesion volume and intact tissue width; Figure S2) or when performing counts on all 38 animals was not practical (axon and axon sub-type counts: Figure 3G-I, Figure S3; SKP-SC orientation analysis: Figure S1).

Determining Lesion Volume, Average Intact Tissue, and Tissue Width.
All three analyses were completed using all longitudinal spinal cord tissue sections (200 μm apart) and the central canal was used to align the spinal cord sections. Tissue was processed with antibodies to GFAP (reactive astrocyte marker) prior to imaging at 5X. Lesion area was defined as GFAP-negative area or GFAP+ area with disrupted/abnormal cytoarchitecture and was manually outlined in each spinal cord section. Cavalieri's principle was applied for volume calculations, i.e., $V = \Sigma$ [area x section thickness x number of sections in each sampling block]. The same sections were used to estimate the amount of intact tissue; we measured the thinnest combination of both 1) the spared rim representing the narrowest width of the rim with GFAP+ tissue with normal

cytoarchitecture on either side of the lesion (as described above); 2) any additional normal-appearing cytoarchitecture resulting from spared tissue bridges. The narrowest width of spared tissue was summed within a section and the average sum from all sections of one animal yielded the mean intact tissue value for that animal.

SKP-SC Transplant Volumes, Transplant Counts, Orientation and Proliferation.
Transplant volumes were completed using all longitudinal spinal cord tissue sections (200 μm apart) with the central canal being used to align the spinal cords and processed with antibodies against GFP, P0, and GFAP. Images were taken at 5X and thresholds were set by the observer to yield an area occupied by the GFP+ SKP-SCs using Sigma Scan software. These GFP+ transplant areas were further subdivided into regions inside the lesion (defined above) versus outside the lesion and converted into transplant volumes using Cavalieri's principle.

The high-survival transplant sub-group (n=5) was used to estimate densities of the SKP-SCs within these transplants. To obtain GFP+ cell counts, sections every 400μm through the entire spinal cord were imaged (n=5) and optical dissector boxes (100μm^2) were randomly placed at a distance of 320um from one another throughout sections containing GFP+ grafts. Confocal Z-stacks were imaged (at 63x) if they contained GFP+ cells and GFP+/Hoechst+ SKP-SCs were counted within the volume of the z-stacks using the optical dissector technique (West M.J. (2012) Basic Stereology for Biologists and Neuroscientists. Cold Spring Harbor, New York: Cold Spring Harbor Laboratory Press). This method is well-established as an accurate way to obtain an average transplant cell density. The resulting GFP+ SKP-SC density was used to estimate the total number of SKP-SCs in the previously measured GFP+ volumes in SKP-SC-treated animals. The volume of SKP-SCs ranged from 0.0006 to 0.23 mm^3 and the average density of cells was $5.325x10^{-4}$ cells/μm^3. In the same set of images, we determined the percentage of GFP+ SKP-SCs that were also P0+, to yield the percentage of myelinating SKP-SCs.

The average orientation of the transplanted SKP-SCs was measured in the SKP-SC sub-group (n=5): three serial sections were selected and single plane images of the GFP+ area were analyzed with ImageJ software (National Institute for Health, USA). Each cell was assigned a vector representing the orientation of the cell and the deviation away from zero (rostral-caudal orientation) was calculated and compared between the rostral, middle and caudal sections of the cord. Cells that were observed in cross section (i.e. orthogonal to the plane of sections) were given a 90° value. The orientation values were compared to a value of 45 degrees (representing a random orientation of the cells in a 2D plane).

An additional quantification of SKP-SC proliferation was performed in three animals (with transplantation estimates >70,000 cells), by counting the GFP+ cells that co-expressed the proliferation marker KI67 at 21 wpi.

GFAP Intensity Analysis.
Analyses was completed using all longitudinal spinal cord tissue sections (200 μm apart) with central canal used to align cords. Intensity profiles of the GFAP immunoreactivity were generated along six (one pixel wide and 320 μm long; 5X primary magnification; Figure 2A-C) lines perpendicular to the lesion edge. The animal averages were then averaged for each group and further broken down according to whether or not this drawn line (extended into the lesion) was directly on SKP-SCs (GFP+), directly on endogenous SCs (GFP-negative, P0+) or directly on cavity (with no SKP-SCs or P0+ endogenous SCs in the vicinity). In each situation, the intensity data was normalized to the far distant rostral intact cord for each given animal to correct for inter-animal variations.

SC Myelination and Non-myelinating SC Analysis.
Analyses was completed using all longitudinal spinal cord tissue sections (200 μm apart) with central canal used to align cords. The overall volume of SC myelin (P0+) was measured using a thresholding procedure as described for the GFP+ transplant volume in 5X images. The volume of P0+ myelin associated with transplant-derived SKP-SCs was estimated by measuring the overlap between GFP+ and P0+ areas on each section and converting those areas to volumes (as described above). All P0+ structures not closely associated with GFP+ SKP-SCs were assumed to be of endogenous SC origin. The myelination state was corroborated with antibodies, including CASPR and the voltage gated potassium channel KV1.2., known markers surrounding the nodes of Ranvier. To examine the non-myelinating SC content of the 29 wpi spinal cord tissue, we used P75NTR immunohistochemistry and conducted a volume estimate using the same methods as for GFP+ and P0+ volume analyses described above on an adjacent set of sections.

Axon Counts.
Two axon analyses were conducted in the three sub-groups (n=5 each). In the first analysis comparing the transplantation groups, for each animal, we counted the number of axons in a single 63X optical plane in five sections spaced 200μm apart, whereby the middle section contained the central canal. Axons were counted when crossing a line spanning the lesion (as defined previously) at the narrowest point of the spinal cord (blue lines; Figure 3A,C,E). In addition, we counted the number of axons, axon subsets, and/or P0+ myelinated axons within the GFP+ SKP-SC bridges at three lines drawn at the rostral (100μm from rostral interface), middle, and caudal (100μm from caudal interface) portions of the GFP+ grafts (yellow lines; Figure 3E) to further determine whether any gradients of axon growth exist, e.g. due to ingrowing supraspinal axons. Axons that intersected with the drawn lines were counted throughout the single 20 μm section using the section with the largest SKP-SC transplant area which happened to be within 200 μm ventral to the central canal. Images for all axon counts were captured at 63X, including TH+ axons, SERT+ axons, CGRP+ axons, axons (βIII tubulin/NF-200), and P0+ axons (βIII tubulin/NF-200/P0+). Axons surrounded by P0+ sheaths were counted to calculate the percentage of myelinated axons within the SKP-SC bridges.

Bladder Analysis.
Wet weight of the dissected bladders was recorded. Bladders were then dabbed dry and a small 3 mm ring-shaped band was cut from the bladder starting at the rostro-caudal midline moving caudally and frozen in Tissue-Tek O.C.T. (Sakura, Netherlands) in an orientation that allowed for transverse sectioning of the bladder wall. Bladders were handled carefully in dissection and preparation to avoid stretching the tissue; also, tissue preparation was performed by blinded experimenters. Four animals were excluded from the bladder analysis due to severe damage to the bladder during tissue processing. Sections were stained for 5 minutes in 0.1% Cresyl Violet and subsequently imaged at 10X. Two sections were measured per animal (2000μm apart), where a one-pixel thick line was drawn through the thickest section of the bladder wall to obtain a mean max wall thickness.

Statistical Analyses

Statistics were calculated using SPSS (IBM; Markam ON, CA). If data met assumptions of normality and homogeneity of variance, groups were compared using the appropriate independent t-test, paired t-test, or a repeated measures (RM) analysis of variance (ANOVA) for two groups and using a one-way ANOVA with a Least Significant Difference *post hoc* test for three groups with data presented as mean ± SEM. If the assumptions of normality and homogeneity of variance were not met: groups were compared using the Kruskal-Wallis (KW) one-way analysis of variance with follow up Mann-Whitney U (MWU)-test for three independent groups and just the Mann-Whitney U-test for two paired groups or a Friedman test with follow up Wilcoxon test for three paired groups and just the Wilcoxon test for two paired groups with data presented as raw values with the median indicated. Correlation analysis was conducted using Pearson's correlation coefficient (parametric) or Spearman's rank correlation coefficient tests (non-parametric). The significance level for all two-tailed tests was $p<0.05$. Trends were reported for two-tailed tests when $p<0.1$ indicative of a significant one-tailed test.

Supplemental References:

Basso, D.M. (2004). Behavioral testing after spinal cord injury: congruities, complexities, and controversies. J Neurotrauma *21*, 395-404.

Basso, D.M., Beattie, M.S., and Bresnahan, J.C. (1995). A sensitive and reliable locomotor rating scale for open field testing in rats. J Neurotrauma *12*, 1-21.

Biernaskie, J., Paris, M., Morozova, O., Fagan, B.M., Marra, M., Pevny, L., and Miller, F.D. (2009). SKPs derive from hair follicle precursors and exhibit properties of adult dermal stem cells. Cell Stem Cell *5*, 610-623.

Fernandes, K.J., McKenzie, I.A., Mill, P., Smith, K.M., Akhavan, M., Barnabe-Heider, F., Biernaskie, J., Junek, A., Kobayashi, N.R., Toma, J.G*., et al.* (2004). A dermal niche for multipotent adult skin-derived precursor cells. Nat Cell Biol *6*, 1082-1093.

Ghilusi, M., Plesea, I.E., Comanescu, M., Enache, S.D., and Bogdan, F. (2009). Preliminary study regarding the utility of certain immunohistochemical markers in diagnosing neurofibromas and schwannomas. Rom J Morphol Embryol *50*, 195-202.

Hamers, F.P., Lankhorst, A.J., van Laar, T.J., Veldhuis, W.B., and Gispen, W.H. (2001). Automated quantitative gait analysis during overground locomotion in the rat: its application to spinal cord contusion and transection injuries. J Neurotrauma *18*, 187-201.

McKenzie, I.A., Biernaskie, J., Toma, J.G., Midha, R., and Miller, F.D. (2006). Skin-derived precursors generate myelinating Schwann cells for the injured and dysmyelinated nervous system. J Neurosci *26*, 6651-6660.

Metz, G.A., and Whishaw, I.Q. (2002). Cortical and subcortical lesions impair skilled walking in the ladder rung walking test: a new task to evaluate fore- and hindlimb stepping, placing, and co-ordination. J Neurosci Methods *115*, 169-179.

Scheff, S.W., Rabchevsky, A.G., Fugaccia, I., Main, J.A., and Lumpp, J.E., Jr. (2003). Experimental modeling of spinal cord injury: characterization of a force-defined injury device. J Neurotrauma *20*, 179-193.

Toma, J.G., McKenzie, I.A., Bagli, D., and Miller, F.D. (2005). Isolation and characterization of multipotent skin-derived precursors from human skin. Stem Cells *23*, 727-737.

Vrinten, D.H., and Hamers, F.F. (2003). 'CatWalk' automated quantitative gait analysis as a novel method to assess mechanical allodynia in the rat; a comparison with von Frey testing. Pain *102*, 203-209.